Reliability of Marine Structures Program

NONLINEAR SHIP LOADS
AND
SHIP FATIGUE RELIABILITY

Alok K. Jha

Supervised by

Steven R. Winterstein

Civil Engineering Department, Stanford University

June 1997

Report No. RMS–26

Department of CIVIL ENGINEERING
STANFORD UNIVERSITY

NONLINEAR SHIP LOADS
AND
SHIP FATIGUE RELIABILITY

Alok K. Jha

Supervised by

Steven R. Winterstein

Civil Engineering Department, Stanford University

June 1997

Report No. RMS–26

Acknowledgments

This study is part of the doctoral work of the author and has been funded by the Office of Naval Research under the supervision of Dr. Peter Majumdar, and grant N00014-96-1-0641, under the supervision of Dr. Roshdy S. Barsoum. Additional financial support has been provided by the industry sponsors of the Reliability of Marine Structures Program of Stanford University. We thank Det Norske Veritas, Hovik, Norway for donating the numerical ship model and the ship analysis program

We gratefully acknowledge these sources of support.

Abstract

Stochastic methods are described here to predict the effects of nonlinear ship loads on fatigue accumulation in random seas. These are found to be capable of predicting the net fatigue damage over many ship response cycles, at a fraction of the cost of direct time-domain analysis. It is also shown how these nonlinear ship load models can be used within a full reliability analysis of ship components. This uses first-order reliability methods to estimate not only the net effect of all uncertainty sources, but also the relative contribution of each (e.g., load vs. material property variability). In our ship load application, nonlinear effects are found to increase the relative impact of load (and wave) modelling and its uncertainty.

The ship load analysis for fatigue is based on a new concept, the "narrow-band transfer function" (NTF) method. The basic idea is to apply the nonlinear time-domain ship load analysis to a limited set of regular, sinusoidal waves. This establishes the narrow-band transfer function; i.e., the ship load amplitude from nonlinear analysis as a function of the wave amplitude and period. Stochastic process theory is used both to select which regular waves (i.e., heights and periods) to use, and to decide how these results should be weighted in predicting load statistics in an irregular sea.

The result is compared with full nonlinear analysis of a specific ship over long simulations of an irregular sea. A ship with relatively flared cross-section is chosen, which shows marked nonlinearity and hence asymmetry in its positive and negative (sag and hog) mid-ship bending moment. The NTF method is shown to accurately predict the results of the long nonlinear simulations. This suggests great reduction in analysis costs: time-domain analysis over many cycles of an irregular sea is replaced

by a limited number of regular wave analyses. Similar methods have been found useful in other ocean engineering contexts; e.g., predicting loads and motions of fixed offshore structures.

Finally, we show a fatigue reliability example for this ship structure where the probability of failure is found by integrating the uncertainties at all three levels: the wave climate, the structural response given the wave climate and the material properties. Here an efficient method is also shown to select the associated design parameters in order to achieve a preselected reliability level.

Contents

List of Tables

List of Figures

Chapter 1

Nonlinear Ship Loads: Stochastic Models for Fatigue Analysis

1.1 Introduction

Fatigue cracking in ship details can lead to much expensive repair and should be considered in design of structural elements. A ship is typically designed to have a service life of about 20 years, during which it undergoes millions of load cycles that may result in fatigue cracks. In general, the fatigue hot spots can be at the ship bottom, the side shell, or in the main deck. A Swedish study conducted on 85 ships (see [26]) for damage due to cracks, deformations, and corrosion suggested that about 70% of the damage was due to fatigue.

Existing recommendations (see [1, 7]) for fatigue analysis and design (outlined in the following sections) either tend to be limited in accuracy of load analysis and hence fatigue damage, or are prohibitive in terms of computational resources. The study here suggests an approach that efficiently uses state-of-the-art nonlinear ship analysis

tools to accurately predict fatigue damage without the heavy computational burden. This method also finds application in fatigue analysis of side shells [13] and in extreme ship-response analysis [35].

Note that this study is part of the doctoral studies of the author and this report has largely been adapted from the author's thesis [16].

1.2 Ship Model

The fatigue reliability studies presented here are demonstrated for ships and in general should be applicable to any offshore structure that responds primarily in a quasi-static manner to the wave loads. We focus here on a monohull ship with flared cross-sections. A body plan and a strip model of this ship are shown in Figure 1.1 and the main particulars of the ship are given in Table 1.1. The cross-section of the ship changes along the length of the ship with flared cross-sections at the ends of ship and box cross-sections towards mid-ship (see Fig. 1.1b). The ship-equipment mass and the ship dead-weight cause nonuniform mass distribution along the ship. A ship moving in the waves is subjected to many kinds of loads: vertical and horizontal bending moments, torsional moments, side shell intermittent water pressures, etc. In this study we consider only the mid-ship vertical bending moments (or equivalent mid-ship bending stresses) as loads on the ship (see Fig. 1.2). The sagging condition causes tensile stresses in the ship bottom, while the hogging condition may extend fatigue cracks in the ship deck. Lateral side shell or torsional loads are not considered in this study; however, the methodology developed here should be equally applicable for these loads as well.

The ship is assumed to be rigid and respond to the wave loads in heave and

Table 1.1: Main Particulars of Ship presented in Fig. 1.1

Specification	Value
Length between perpendiculars	166m
Beam	24.65m
Draught	8.85m
Weight	2×10^5 kN
Waterplane Area	2.84×10^3 sq.m

pitch degrees of freedom. We use a strip theory analysis program NV1418 [5, 11] to perform a time domain estimation of the ship loads. This program is limited to head seas loads. While no slamming or water on deck are considered, we integrate the water pressures to the exact wetted surface to find the rigid body forces on the ship and the resulting mid-ship bending moments. The pressure integration to the instantaneous wetted surface, and the flared hull cross-section, contribute primarily to the nonlinearity in the ship loads. The sag bending moments are typically larger than the hog bending moments, for example. A linear analysis, on the other hand, is based on the assumptions of small ship oscillations and, consequently, the bending moments do not show any nonlinearity (see Sec. 1.4.1).

1.3 Stochastic Fatigue Analysis

A general approach to fatigue analyses in reliability-based fatigue design, is to use available fatigue test data [29]. Typically, in fatigue tests a specimen undergoes constant amplitude S cyclic loading and the number of cycles N to "fail" is recorded. A linear fit to $\log S$ vs. $\log N$, called an S–N curve, provides the following relation:

$$N = CS^{-b} \tag{1.1}$$

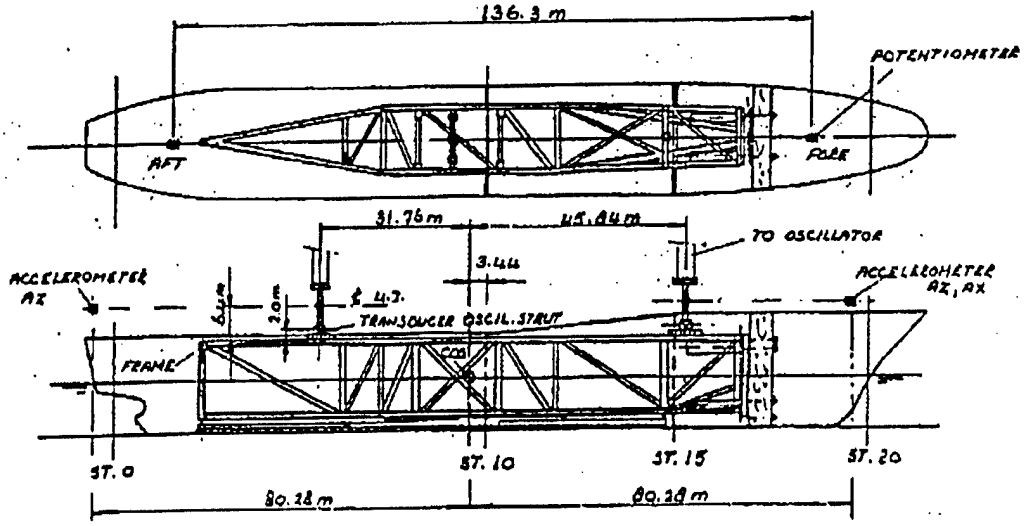

(a) Body Plan

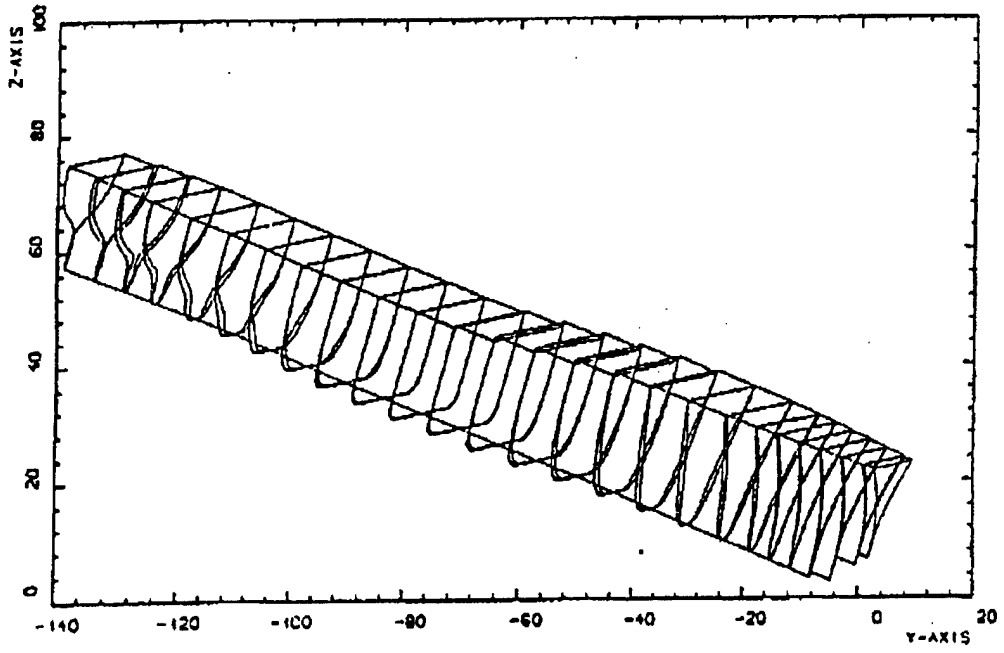

(b) Strip Model

Figure 1.1: Model of monohull ship that will be analyzed using strip theory

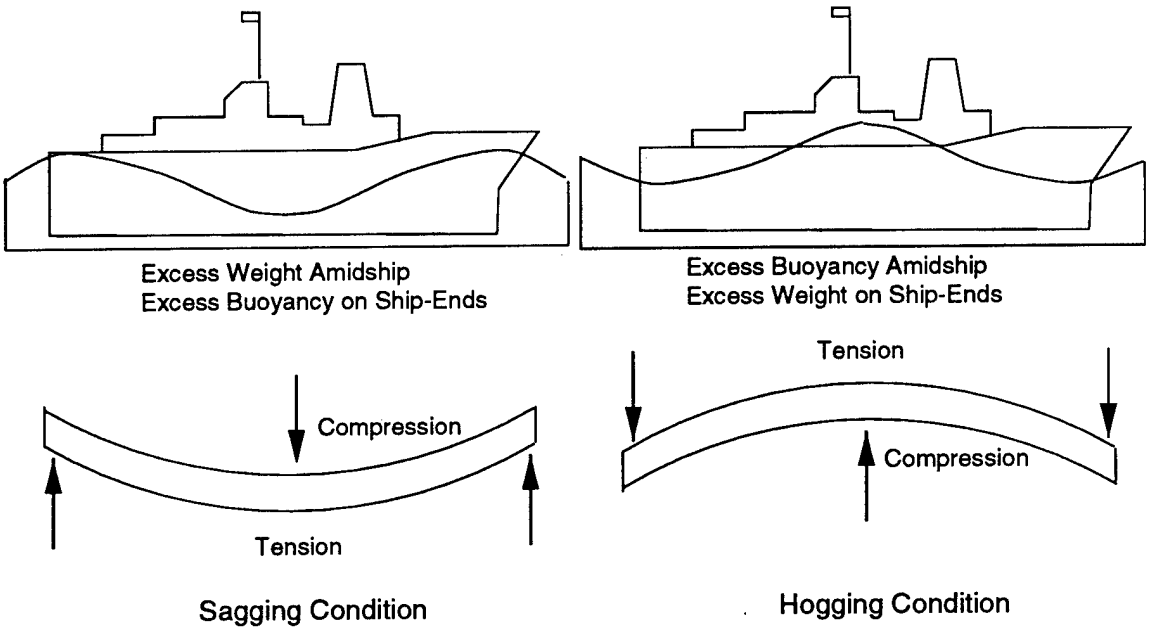

Figure 1.2: Sag and Hog Bending Condition of Ship in Waves

where C and b are the intercept and the slope of the fitted curve. This relation gives the mean number of stress loading cycles N with amplitude S that a fatigue specimen can tolerate before failing [12]. The material factor C, in general, shows a large scatter (coefficient of variation on the order of 50 to 60%). Typical values of the exponent b for steel material may be 3–6, and may be as high as 7–10 for composite materials. Values of S–N parameters for offshore structure materials and their uncertainties can be found in various literature, including API [2] and SSC reports [26] among others.

For real structures, however, the loading is random in nature and we need to relate the random stress amplitudes to the number of cycles to fail. The Palmgren-Miner linear cumulative damage hypothesis [12] may be used to apply the S–N relation to estimate the fatigue damage from a random stress history. Linearity of this hypothesis lies in the absence of any sequence effects of the random stresses. The hypothesis

estimates the mean damage due to a single stress cycle with amplitude s to be $1/N_s$, where $N_s = Cs^{-b}$ is the mean number of cycles to fail at stress amplitude s. Thus, according to this hypothesis, the mean damage $\overline{D}$ in N cycles from a random stress history, whose stress amplitudes have probability density function $f_S(s)$, is

$$\overline{D} = \int_0^\infty \frac{N f_S(s)}{N_s} ds = \frac{N}{C} \int_0^\infty s^b f_S(s) ds = (N/C) E[S^b] \tag{1.2}$$

where $N = \nu T$ is the number of stress cycles in a given duration T due to a stress cycle rate ν. The mean value of the b-th power of S can be found once its distribution $f_S(s)$ is known. Note that $E[S^b]/C$ is the mean damage per cycle, and $\nu E[S^b]/C$ is then the mean damage rate (damage per unit time) which when multiplied by a duration T gives the mean damage $\overline{D}$ in T. For high-cycle rate applications, variations about the mean damage per cycle will average out quickly, so that the actual damage in time T can be quite accurately approximated by the mean damage $\overline{D}$ in time T. The following section outlines a few approaches typically used to identify $f_S(s)$.

1.3.1 Existing Approaches to Fatigue Analysis

This section briefly summarizes the existing approaches to model the distribution of the stress load cycles. According to existing guidelines for fatigue analysis (for example, [7]) we need to formulate the long-term stress distribution $f_S(s)$ for the structural component. Some ways to find it are:

1. Simplified analysis in conjunction with ship guidelines:

$f_S(s)$ can be modeled as a Weibull distribution:

$$P[S > s] = \exp\left[-(s/\beta)^{\alpha}\right] \tag{1.3}$$

where α and β are the shape and the scale parameters of the distribution. The b-th moment of a Weibull S is given as

$$E[S^b] = \beta^b \Gamma\left(1 + b/\alpha\right) \tag{1.4}$$

where $\Gamma(u) = \int_0^\infty t^{u-1}e^{-t}dt$ for $u > 0$ is the Gamma function.

Simple empirical rules (or more refined long-term analysis) may be used to find α. For example, Ref. [7] suggests $\alpha \approx 2.21 - 0.54\log_{10}(L)$ for fatigue analysis of deck longitudinals, where L is the ship length in meters. The second parameter β is then found from an estimated stress value at a known fractile in the distribution. This stress is found by performing a detailed analysis due to an assumed wave cycle that is likely to result in stresses at the desired fractile. Although this method permits a quick and simple fatigue analysis scheme, drawbacks do exist. For example, β is tuned to a single stress analysis and may be sensitive to the choice of the stress return period. This can, of course, be resolved by tuning β to different stresses and studying the consequence on fatigue damage estimates. Another problem that still exists, however, is how do we select a wave (or the wave parameters: height H and period T) that should result in stresses with a desired return period? If the response given a wave with height H were deterministic, and if T varied deterministically with H, then the return period of the wave would exactly be the return period of the resulting stress. In general, the response given a wave is random (also T given H is

random) and hence the difficulty in identifying the wave.

2. Long-term stresses based on long-term climate conditions:

The long-term wave climate is divided into short-term climatic conditions called seastates. The duration of a seastate, typically 1–6 hours, reflects the time in which the waves can be assumed to be stationary. Parameters typically chosen to characterize a seastate are the significant wave height H_s, defined to be four times the wave elevation standard deviation σ_η, and the peak spectral period T_p. A ship response analysis in irregular waves (see Sec. 1.4) could then provide the stresses as a function of H_s and T_p. This leads to the long-term stress distribution

$$f_S(s) = \iint f_{S|H_s,T_p}(s|h_s,t_p)\; f_{H_s,T_p}(h_s,t_p)\; dh_s\, dt_p \tag{1.5}$$

where $f_{S|H_s,T_p}(s|h_s,t_p)$ is the conditional probability density function of stresses given H_s and T_p, and $f_{H_s,T_p}(h_s,t_p)$ characterizes the long-term joint probability density of the seastate parameters. Such joint distributions, characterized for many ship routes around the world, can be found in the literature, for example see Ref. [8]. Note the stress cycle rate $\nu(h_s,t_p)$ may also be a function of the seastate parameters h_s and t_p. In this case, one needs to consider a weighted form of $f_s(s)$ above; e.g.,

$$f_S(s) = \frac{\iint \nu(h_s,t_p) f_{S|H_s,T_p}(s|h_s,t_p) f_{H_s,T_p}(h_s,t_p)\; dh_s\, dt_p}{\iint \nu(h_s,t_p) f_{H_s,T_p}(h_s,t_p)\; dh_s\, dt_p} \tag{1.6}$$

Alternatively, with normalized damage (per cycle) given by S^b, long-term mean damage must consider not just $E[S^b|H_S,T_P]$ but more generally the mean damage $\nu(H_S,T_P)E[S^b|H_S,T_P]$ per unit time (as in section 1.5).

An alternative approach (see, for example, API [2]), would be to use the local

wave heights (wave height H in a single wave) to characterize the wave climate and relate the stresses directly as a function of the wave height H. $f_S(s)$ then based on a long-term distribution of the local wave heights $f_H(h)$ is

$$f_S(s) = \int f_{S|H}(s|h) f_H(h)\, dh \tag{1.7}$$

in which $f_{S|H}(s|h)$ is the probability density of stresses S given the local wave height H. This method does not explicitly assume dependence of stresses on the wave periods.

1.4 Ship Response Analysis Methods

This section discusses different methods to perform a ship response analysis to find the stresses given the climate conditions. These methods differ in the complexities of the hydrodynamical and mechanical models used to perform the analysis. For example, a linear analysis (see below) is based on small ship oscillations, while a 2-D strip theory, studied here, accounts for the ship position in the wave and integrates the water pressure to the exact wave surface. This approach can be extended to perform a 3-D analysis accounting for fluid-structure interaction effects.

- **Linear Ship Load Analysis**: A linear analysis is used to find the Linear Transfer Function (LTF) that relates waves to ship loads for a ship traveling at a given speed. In this study, a strip theory is used to estimate the linear loads by integrating the water pressures to the mean water level [33]. In a short-term seastate (typically of 1 to 6 hours duration), the ship load is assumed to be Rayleigh distributed with the load standard deviation σ (and stress cycle rate) found from the spectrum of linear loads. A weighted Raleigh distribution across

all seastates accounting for different ship speeds, and the long-term distribution of the seastates, may then in turn be used to directly find $E[S^b]$, or to calibrate an equivalent Weibull model, which may then used to find $E[S^b]$. Although still a linear analysis, this approach includes the frequency content in the load estimation and is computationally inexpensive.

- **Nonlinear Ship Load Analysis**: State-of-the-art 3-D nonlinear ship analysis tools like SWAN [18,27], Lamp [19,20], and USAERO [4], for example, can be used to estimate the global loads. In this study, we use a 2-D strip theory [5,11], as described in Sec. 1.2, to estimate the loads on a ship, and then find the resulting fatigue damage. Such tools perform increasingly complex nonlinear analyses to gain accuracy in the load estimates; the computational burden increases in intensity, however. We need to use these expensive tools minimally to predict fatigue damage with the least computational burden.

In the following section, we demonstrate the need to perform a nonlinear load analysis, instead of a linear one, to estimate fatigue damage, and then propose a new approach to perform such a nonlinear damage estimate.

1.4.1 Comparison of Ship Response from Linear and Nonlinear Analyses

We compare the ship loads (mid-ship bending moments) from linear and nonlinear analyses in an irregular sea to emphasize the effects of nonlinearities in the loads. The example sea chosen here is described by a JONSWAP spectrum with significant wave height $H_s = 5$m, spectral peak period $T_p = 10$s, and peakedness factor $\gamma = 3.3$. The ship is assumed to be traveling at a speed of 10 knots (=5.144 m/s) into a head

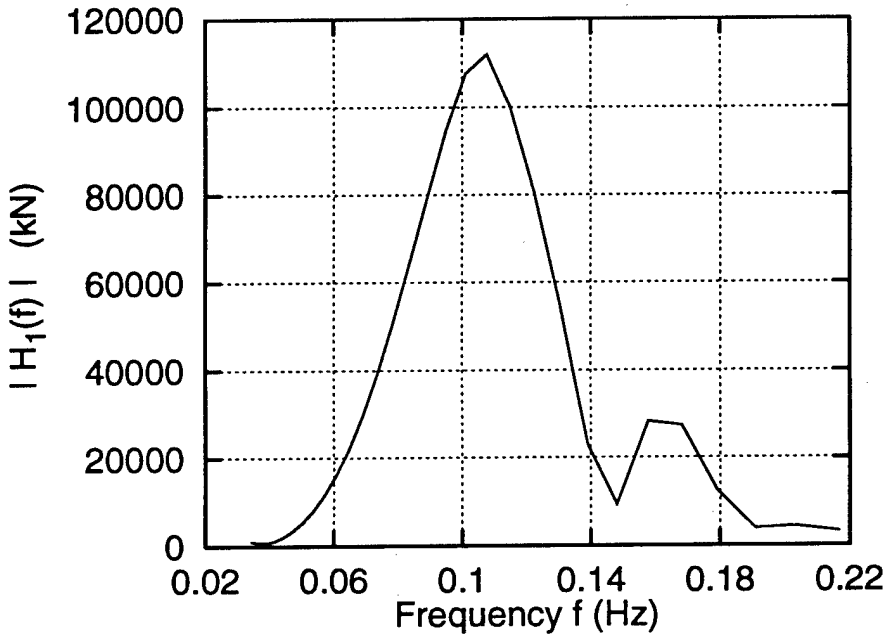

Figure 1.3: Linear Transfer Function for Mid-ship Bending Moment Response

sea. The linear bending moments are estimated from a linear transfer function (see Fig. 1.3) relating the wave elevation process $\eta(t)$ to the mid-ship bending moments. Note that the linear transfer function peaks at about $f = 0.1$Hz, or wavelength = 156 m (from linear dispersion relation). This is close to the ship length and so this chosen sea reflects a ship-length tuned sea. The nonlinear history is estimated from NV1418 using a 2-D strip theory [5, 11]. Partial mid-ship time histories of the Gaussian waves, the linear bending moments, and the nonlinear bending moments from an hourly analysis are shown in Figure 1.4.

The sag bending moments (positive peaks) are typically larger than the neighboring hog bending moments (absolute value of negative peaks) in the nonlinear load history, while the bending moments are symmetrically distributed in the linear load history. Note that the range bending moment (=sag+hog) is also, on average, smaller

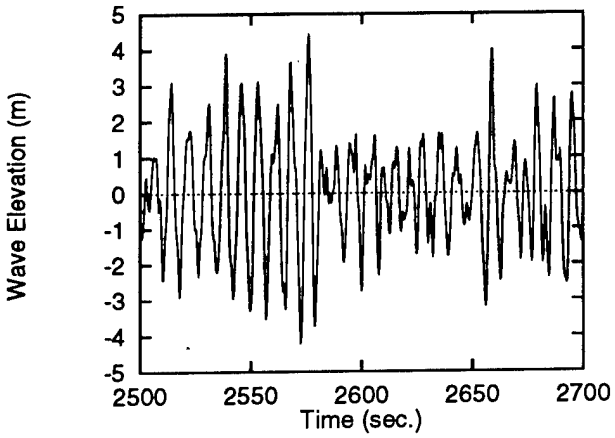

(a) Wave History

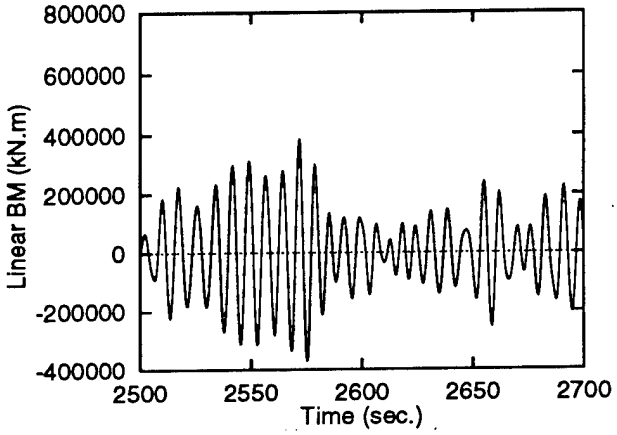

(b) Linear Response History

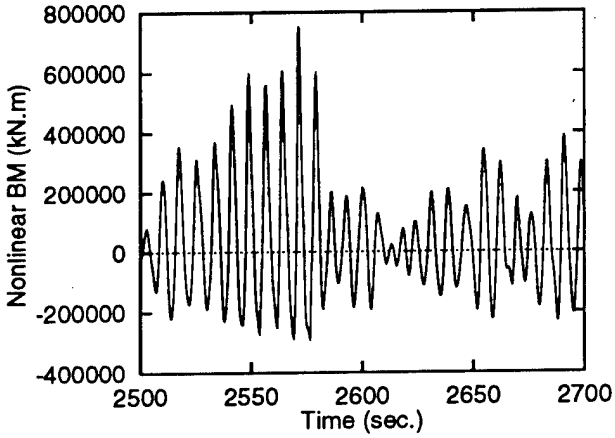

(c) Nonlinear Response History

Figure 1.4: Partial wave and response histories at mid-ship

Table 1.2: Statistics of Ship Load History

	Linear Analysis	Nonlinear Analysis
Mean μ	0	0.21×10^5 kN.m
Sigma σ	1.06×10^5 kN.m	1.36×10^5 kN.m
Skewness α_3	0	0.6
Kurtosis α_4	3.0	3.4

from the linear analysis. The history statistics of the two analyses are given in Table 1.2. The skewness of 0.6 in the nonlinear history provides a measure of the marked asymmetry between the sag and hog bending moments. Note also that standard deviation of the linear history is approximately 30% smaller than that of the nonlinear analysis. This may be due to the limitation of the small oscillation assumption in linear theory, which thereby ignores the increasing nonlinearity as the length of the waves approach the ship length (see Fig. 1.3). Owing to the smaller sag bending moments from linear theory and the resulting smaller ship keel (bottom) tensile stresses, the rate of crack growth will be considerably underpredicted by linear theory.

Fig. 1.5 compares the fatigue damage from the linear analysis to that from the nonlinear analysis. The linear fatigue damage D_L in duration T_d is (see Eqn. 1.2):

$$D_L = T_d \nu_0 E[S^b] \tag{1.8}$$

in which ν_0 is the stress cycle rate and $E[S^b]$ can be found from Eqn. 1.4, where for a Rayleigh stress (due to linear theory) distribution $\alpha = 2$ and $\beta = \sqrt{2}\sigma$. Note that in Eqn. 1.8, we have ignored the S–N coefficient C and the section-modulus in converting bending moments to stresses. These are treated as material constants and will cancel out when looking at ratios of damage estimates.

The fatigue damage D_{NL} is estimated from 20 hours of simulated nonlinear response in irregular waves in this seastate and is given as

$$D_{NL} = T_d \nu_0 E[S^b] = \sum_{i=1}^{N} S_i^b \tag{1.9}$$

in which N is the total number of stress cycles, and S_i, $i = 1 \ldots N$ are the sag, hog or range stresses seen in 20 hours. In this study, we will refer to D_{NL} as the "exact" damage estimate and ask how close are the damage estimates from simpler prediction models. A comparison of linear to nonlinear fatigue damage shows that the sag-induced fatigue damage can be considerably underpredicted by the linear model. Linear hog damage is closer to the nonlinear hog damage, since the predicted hog bending moments from linear theory seem close to those from the nonlinear analysis (see Fig. 1.4). Recall that hog bending moments occur due to wave crests near midship (see Fig. 1.2) where the cross-section is box-like, and so there, indeed, is potential for linear theory to correctly predict hog bending moments. As a net effect of sag and hog, the range fatigue damage is also underpredicted by the linear model, although, to a lesser extent than the sag underprediction.

As seen in Fig. 1.5, a nonlinear analysis of sag-induced fatigue for a flared ship can provide larger fatigue damage estimates than a linear analysis, particularly for large values of the fatigue exponent b. Such a nonlinear analysis is computationally intensive, however, and is thus an expensive solution to find accurate damage estimates. In this study, we look at an alternative method to estimate damage from nonlinear ship loads. This method is referred to here as a "Nonlinear Transfer Function" (NTF) model, as described in Section 1.5.

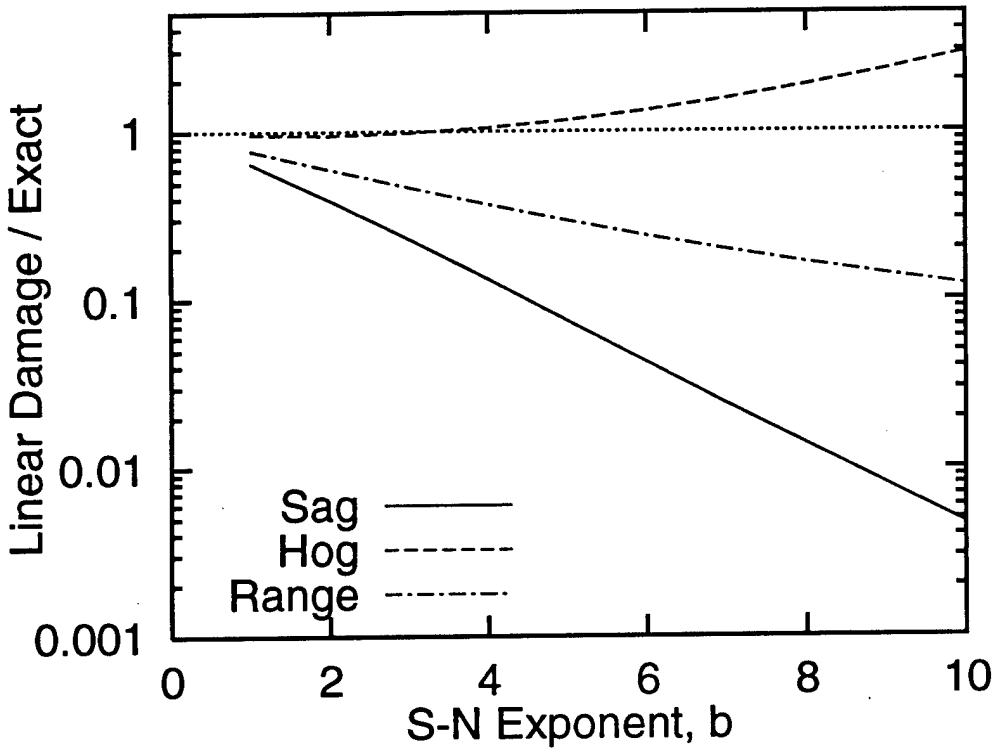

Figure 1.5: Comparison of fatigue damage from linear and nonlinear analysis for sag, hog and range bending moments

1.5 Proposed NTF Approach

In this study, we propose an NTF model to estimate ship loads and the resulting fatigue damage. In this model, we apply the expensive nonlinear analysis to find stresses for only a limited, carefully selected set of wave amplitudes and frequencies. As the force analysis may be rather complex, a minimal set of amplitude and frequency values is chosen. The results are then appropriately weighted to reflect the amplitude-frequency distribution of actual random waves. The numerical set of stress values for the selected waves represents what we call the "Nonlinear Transfer Function".

The stresses from this limited set of waves, in combination with their associated probability weights, can be used to estimate the resulting fatigue damage estimate. This cheaply estimated fatigue damage is intended to approximate the relatively expensive, exhaustively simulated damage from a complete irregular nonlinear time domain analysis.

We will first confirm out theoretical distributions of the wave amplitudes and frequencies by comparing the results with simulated random waves. We then investigate the adequacy of such waves in successfully predicting the load statistics. This is done by comparing the regular wave results to a corresponding complete random wave analysis.

We test this model by comparing, in this example seastate ($H_s = 5$m, $T_p = 10$sec), the predicted damage to the exact damage from Eqn. 1.9. Linear theory predicts this seastate to be about the most damaging seastate for an S–N exponent $b = 4$ (chosen to reflect steel materials), as explained below.

In linear theory, the ship load (stress) process X is assumed to be Gaussian and hence the sag (or hog) bending moments (or stresses S) are Rayleigh distributed. The mean damage rate $E[D_r|H_s, T_p]$ given H_s and T_p can then be written (from Eqn. 1.8) as

$$E[D_r|H_s, T_p] = E[\nu S^b|H_s, T_p] = \nu(H_s, T_p)\left(\sqrt{2}\sigma(H_s, T_p)\right)^b \Gamma(1 + b/2) \qquad (1.10)$$

where $\sigma(H_s, T_p)$ is the standard deviation and $\nu(H_s, T_p)$ is the cycle rate of process X, both of which are seastate-dependent. The total long-term damage D_{LT} is

$$D_{LT} = T_d \iint E[D_r|H_s, T_p]\, f_{H_s,T_p}(h_s, t_p)\, dh_s\, dt_p \qquad (1.11)$$

in which the integrand $E[D_r|H_s,T_p]\ f_{H_s,T_p}(h_s,t_p)$ is the contribution to D_{LT} from each seastate (sometimes called the damage density) and is shown in Fig. 1.6 for a joint distribution model of H_s, T_p, representing Northern North Sea data as suggested in [14]. The damage density is largest in approximately $H_s = 5$m, $T_p = 10$sec., and because large linear loads probably imply large nonlinear loads, as seen in Fig. 1.4, we choose this example seastate to study the accuracy of the NTF model. Note however the modeling errors may be greater in this seastate than in D_{LT}; we use this seastate to most severely test the NTF model and not to suggest typical errors to be expected in estimates of D_{LT}, the long-term damage.

1.5.1 NTF Modeling Issues

As proposed, the idea of the NTF model is to find reliable estimates of fatigue damage from a limited set of wave runs rather than performing expensive nonlinear analyses across all the climate conditions. The key issues in the development of this model are:

- **Selection of waves from theory**: The selection of wave parameters (here the wave height and the wave period) and their associated probabilities of occurrence is based on stochastic theory. Each of the selected waves is stepped through the nonlinear time domain analysis to estimate the ship loads. The questions that arise here are: how accurately does this stochastic theory characterize the waves? And how many waves should we choose to robustly estimate fatigue damage? We will address the first issue in Section 1.5.2 in more detail. The second issue will be discussed by choosing different numbers of selected waves and then comparing the resulting fatigue damage estimates to simulated data.

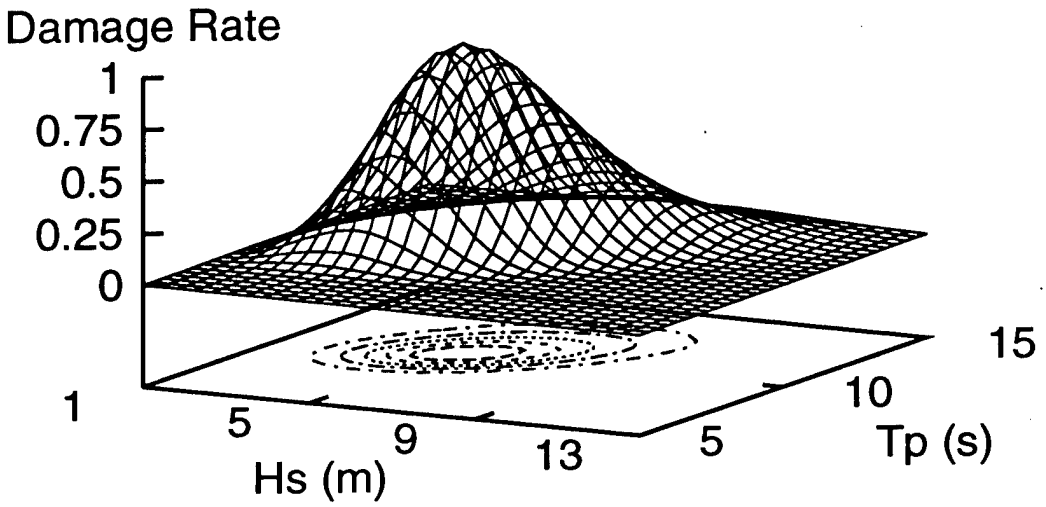

Figure 1.6: Damage density from a linear analysis vs. long-term seastate parameters. The damage rate shown has been normalized by the largest value.

- **Inclusion of spatial wave effects**: In order to include the spatial wave effects, stepping the ship through just one wave cycle may not suffice in estimating the ship loads. This is because at any given time instant the loads depend on the spatial waves across the ship, and on the position of the ship in these waves. We may need to include such spatial effects in the limited wave runs. We hope to achieve this by constructing "most-likely" side wave cycles around each of the selected waves, and then stepping the ship through this triplet to find the resulting ship loads. We address this issue further in Section 1.5.3.

1.5.2 Selection of Waves from Stochastic Theory

A sinusoidal wave can be defined by two parameters, a wave height H and a wave period T. We verify theoretical distributions of H and T with simulated random waves. For waves in an irregular time histories (see, for example, Fig. 1.4a), we select H's and T's from all the wave cycles; a wave cycle is defined as the wave surface between two successive mean-upcrossings of the wave surface. H is the elevation difference between the highest and the lowest points in a wave cycle and T is the time duration between the mean-upcrossings of a wave cycle. Note that this definition of wave cycle, and corresponding H and T, is introduced here simply to permit critical comparison of separate parts of the NTF model prediction – e.g., $f(H,T)$ and $D|H,T$. These precise definitions do not effect the actual calculation of the nonlinear damage D_{NL}, nor of its estimate D_{NTF} from the NTF model.

Wave Heights from Theory

The wave heights of the selected waves are sampled from the Forristall [10] distribution which is an empirical distribution fitted to observed ocean wave heights. For the Gaussian seastate we are considering (represented by a JONSWAP spectrum with $H_s = 5$ m, $T_p = 10$ sec., and $\gamma = 3.3$), Figure 1.7 shows a comparison of 20 hours of simulated wave heights to the Forristall distribution and the Rayleigh distribution of wave heights. The cumulative distribution function (CDF) of the wave heights H is given as

$$F_H(h) = \mathrm{P}[H < h] = 1 - \exp\left[-\frac{(h/\sigma_\eta)^\alpha}{\beta}\right] \tag{1.12}$$

where σ_η is the standard deviation of the wave elevation process $\eta(t)$, and $\alpha = 2$, $\beta = 8$ for the Rayleigh distribution and $\alpha = 2.126$, $\beta = 8.42$ for the Forristall distribution (from empirical fits). Note that the Rayleigh distribution is a theoretical distribution for a narrowband Gaussian $\eta(t)$, and to the degree $\eta(t)$ is not narrowband, the Rayleigh distribution will tend to overestimate wave height fractiles with respect to simulated Gaussian behavior. In Fig. 1.7, the Rayleigh distribution indeed overpredicts wave heights, while the Forristall distribution offers a closer fit to the simulated wave heights. Similar comparisons of the Forristall model with simulated second-order waves were also found in the wave studies conducted in Reference [15]. We will choose the Forristall model to generate the wave heights for the NTF model.

Theoretical Wave Periods given Wave Heights

Given the wave height H, we predict statistics of the wave period T for the sinusoid from the Longuet-Higgins conditional distribution [22–24, 35] of wave periods given wave heights. This distribution, based on envelopes of narrowband processes, specifies a truncated normal distribution of wave frequencies $\Omega = 2\pi/T$ given the wave amplitude $a = H/2$ as

$$P[\Omega > \omega | a] = \frac{\Phi\left[\frac{a(\overline{\omega}-\omega)}{\sigma_\eta \overline{\omega}\Delta}\right]}{\Phi\left[\frac{a}{\sigma_\eta \Delta}\right]} \tag{1.13}$$

where $P[\Omega > \omega|a]$ is the probability that Ω exceeds a specified ω value given a and $\Phi()$ is the standard normal CDF. $\overline{\omega} = \lambda_1/\lambda_0$ is a mean wave frequency in terms of the wave spectral moments $\lambda_i = \int \omega^i S_\eta(\omega)\, d\omega$. $\sigma_\eta = \sqrt{\lambda_0}$, and $\Delta = \sqrt{\lambda_0\lambda_2/\lambda_1^2 - 1}$ is a unitless spectral bandwidth measure. For example, $\Delta = 0.42$ for a Pierson-Moskowitz spectrum, and decreases from this value for a JONSWAP spectrum with

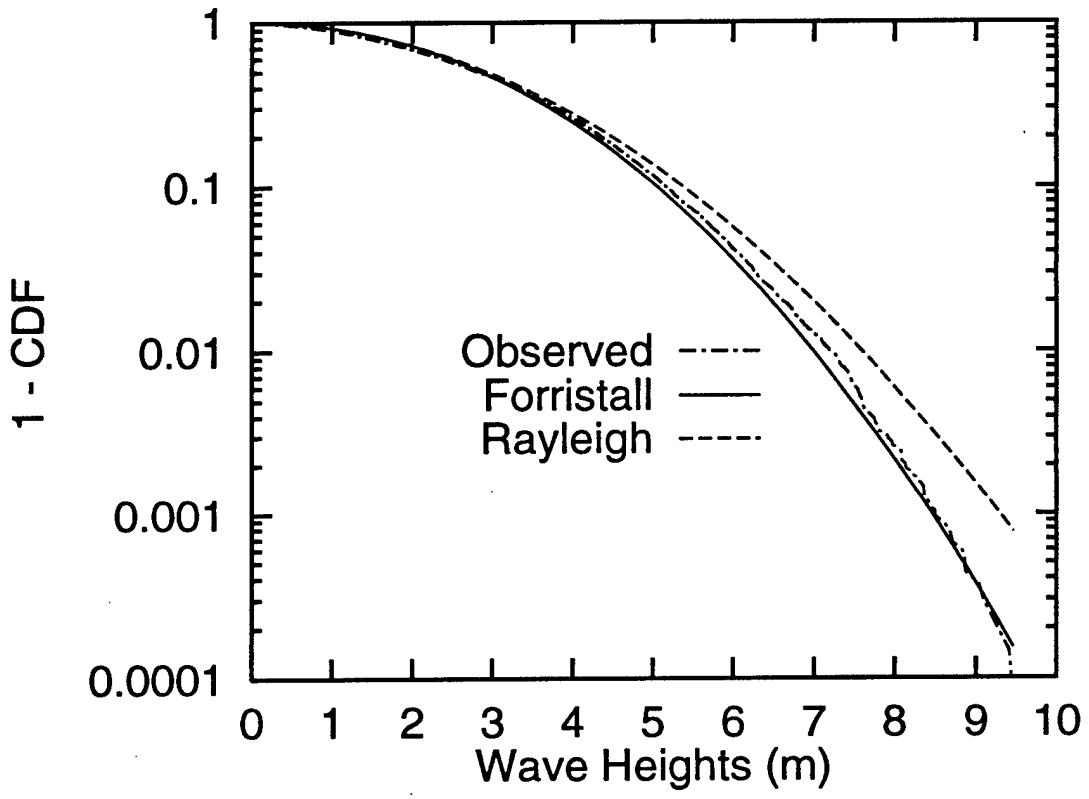

Figure 1.7: Comparison of simulated wave heights to Forristall and to Rayleigh distributions

$\gamma > 1$. Similar models for the conditional distribution have been proposed by Canavie et al. [6] and Lindgren and Rychlik [21]; however, these require at least the fourth spectral moment, which is not generally available for wave spectra and so we propose not to use these models for the fatigue analysis studies. In this study, instead of the central period we take $\overline{T} = 0.92T_p$ (e.g., [25]) and with this modification we will henceforth refer to this conditional wave period distribution as a "modified" Longuet-Higgins distribution. Note that $\overline{T} = 0.92T_p$ seems to match asymptote wave period of the data, while the central period is smaller than this asymptote wave period. The asymptotic conditonal mean wave period is larger than the central period due

to bandwidth effects present in the data. Recall that the original Longuet-Higgins theory is based on narrow-band assumptions. For the example seastate, we find $T_c = 2\pi/\overline{\omega} = 8.35$ sec, while $\overline{T} = 0.92T_p = 9.2$ sec. and matches the asymptotic conditional mean quite closely (as we show next).

To select wave periods in the NTF model, we can relate the frequency fractile ω_p for a given a in the Longuet-Higgins model to the requested probability p. This is done by setting Eqn. 1.13 equal to $1-p$

$$\frac{\omega_p}{\overline{\omega}} = \frac{\overline{T}}{T_p} = 1 - \frac{\sigma_\eta \Delta}{a} \Phi^{-1} \left[(1-p) \Phi \left(\frac{a}{\sigma_\eta \Delta} \right) \right] \tag{1.14}$$

We compare 20 hours of simulated wave period in this example seastate to the wave periods from this modified Longuet-Higgins model. Figure 1.8 shows a comparison of the 16-, 50- (median), and 84- percentile values of wave periods from simulation to those predicted from Eqn. 1.14. For wave heights greater than 3 meters the modified Longuet-Higgins model offers a reasonable approximation to simulated wave periods at the median values and also at the 16 and 84 percentile values of the conditional distribution. For small wave heights, the theoretical wave periods are larger than the simulated periods; however, there is negligible contribution to fatigue damage from these small-height waves, and so, from a fatigue damage standpoint, the modified Longuet-Higgins model appears to offer a satisfactory approximation to the conditional distribution of wave periods given a wave height.

Finally, given a count of the waves to be selected, the choice of wave heights and wave periods given wave heights could, for example, be based on quadrature points. Say, 30 waves are to be selected, as will be used in this study later on. We may mesh the H–T space, so that we have 10 different H values and 3 different T values per H value adding up to 30 waves. We could first select 10 standard normal variables u

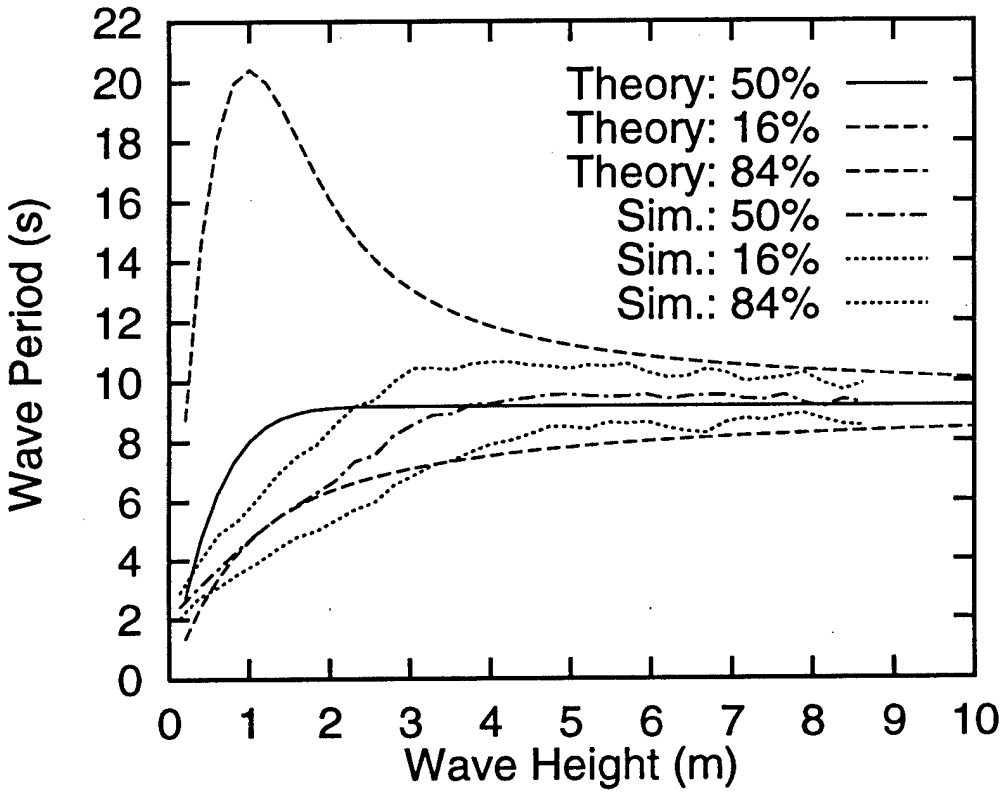

Figure 1.8: Simulated wave period vs. modified Longuet-Higgins wave period

at Gauss quadrature points and then transform these to H values according to the fractile p of u

$$H = \beta[-\log(1-p)]^{1/\alpha} \tag{1.15}$$

Given an H value, we can use Eqn. 1.14 to similarly obtain three T values at 16, 50 and 84 fractiles, for example. The joint occurrence probabilities of the H–T pairs can then be easily found from weights associated with H quadrature points (=P$[U = u_i]$) and from the conditional fractiles of $T|H$.

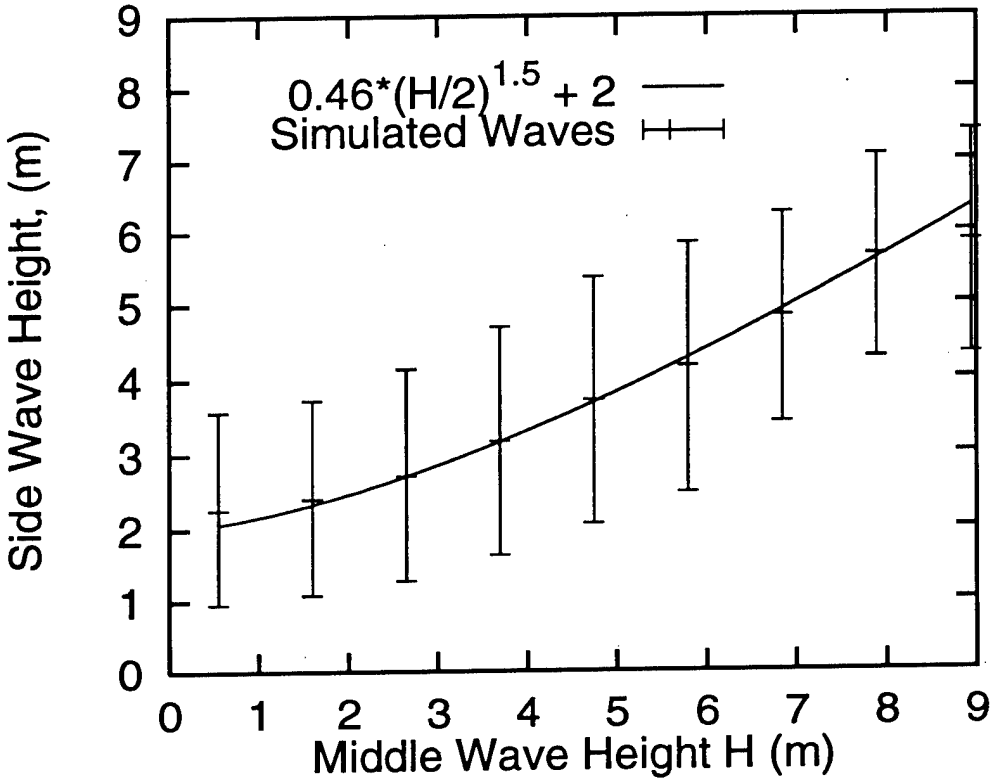

Figure 1.9: Relation of side wave height to middle wave height

1.5.3 Selection of Side Wave Parameters

Since a Gaussian sea has no horizontal asymmetry (reversing a Gaussian history does not change the history statistics), we assume the wave periods and the wave heights of the side waves to be the same. This results in a symmetric wave triplet. Let H_0 and T_0 denote the wave height and wave period of the side waves, respectively, and H and T denote the height and period of the middle wave, respectively (see Fig. 1.10). For the 20 hours of simulated Gaussian waves, we empirically relate $E[H_0|H] = 0.46(H/2)^{1.5} + 2$ as shown in Fig. 1.9. This figure shows the mean, and mean$\pm$ 1 standard deviation of H_0 given various H values in the wave history. Note

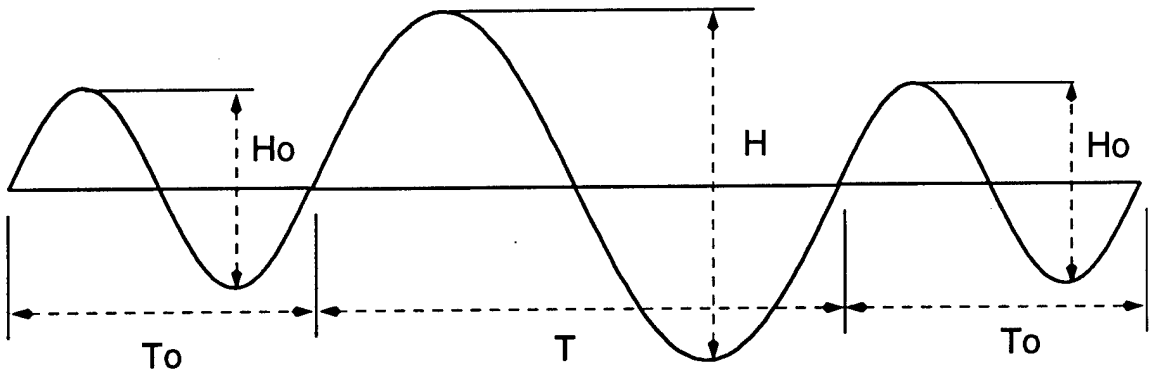

Figure 1.10: Construction of Wave Triplet for NTF Load Prediction

however that this empirical result is seastate-specific. Parametric study across a grid of $H_s - -T_p$ seastates could afford more general results. Alternatively, one may seek analytical results through probability theory. For example, linear regression suggests that

$$E[H_0|H] = m_H + \rho_{H,H_0}(H - m_H) \tag{1.16}$$

Values of the mean wave height, m_H, and the correlation ρ_{H,H_0} between successive heights, can be estimated by random vibration theory.

For the Gaussian wave history, we find that T_0 has negligible correlation with T in this seastate, so we let T_0 given H_0 be the median period from the modified Longuet-Higgins model, without conditioning the choice of T_0 on T. Finally, we construct a wave triplet with three sinusoids in succession (see Fig. 1.10), where H_0, T_0 are the side wave parameters and H, T are the middle wave parameters.

1.6 Predicted NTF Fatigue Damage vs. Data

In this section, we will predict fatigue damage from the NTF model and compare it to exact damage found from 20 hours of simulated stresses. Recall that the simulated stresses are obtained from the nonlinear ship response analysis of 20 hours of Gaussian waves. This analysis is done in a seastate with $H_s = 5$m and $T_p = 10$sec. For the NTF model, we will start out by predicting damage from 30 single sinusoidal waves, and investigate the necessity of imposing side waves on each of these 30 waves. We will then study the accuracy of predicted damage from a reduced set of waves, for example, 15 waves instead of 30 waves.

For the NTF prediction, we select 30 waves (see Fig. 1.11) as the wave set to estimate the mid-ship bending moments. 10 equi-spaced wave heights are chosen for waves, with the maximum H value arbitrarily assumed at 10^{-6} exceedance probability (H with return period of approximately 1 in 1000 hours) according to the Forristall distribution [10]. This return period for H has been arbitrarily chosen to include large rare wave heights as well. We find the weights associated with these 10 H values from the Forristall distribution. Given the H values, the middle wave periods T are chosen to be at 16, 50 (median) and 84 percentile values according to the modified Longuet-Higgins distribution and are found from Eqn. 1.14 using p=0.16, 0.5 and 0.84, respectively. In general, we could increase the number of waves in the set to gain greater accuracy in the predicted results; however, as demonstrated in the following sections these 30 waves seem to represent the simulated bending moment statistics adequately. For each wave height, the three selected wave periods were chosen to have equal probability weights of 1/3 each. Finally, the marginal weights of H can be multiplied with the conditional weights of $T|H$ to find the joint weights p_j of the 30 H and T pairs.

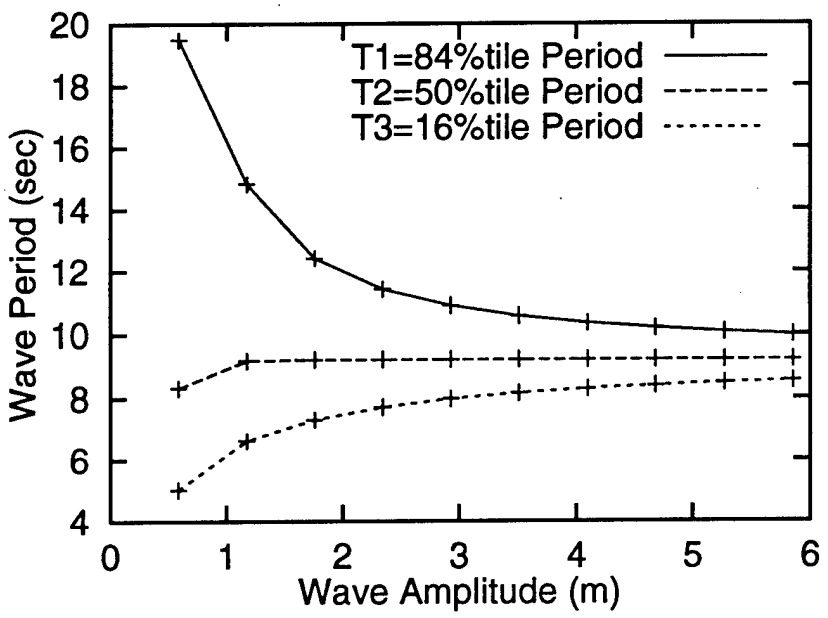

Figure 1.11: Wave heights and periods for the 30 waves used in the NTF model

Let $N_p = 30$ denote the number of waves used to mesh the H-T space. Thus, the H-T space can be divided into N_p cells centered around each of the selected H-T pairs. Let p_j $(j = 1 \ldots N_p)$ denote the probability of "falling" in the jth cell. The p_j values can also be understood as the joint weights associated with the N_p H-T pairs. The NTF predicted fatigue damage D_P from the analysis using $N_p = 30$ waves, then, is

$$D_P = T_d \nu E[S^b] = \sum_{j=1}^{N_p} n_j S_j^b \quad ; \quad n_j = N_w p_j \tag{1.17}$$

where S_j is the predicted ship load, n_j is the predicted number of wave cycles for the jth H–T pair, and N_w is the total number of predicted wave cycles in duration T_d. Since the ship is moving into the waves the number of wave cycles encountered by the ship and the resulting number of stress cycles depends on the speed of the ship [9].

The number of wave cycles $N_w = \nu_{\text{enc}} T_d$, where ν_{enc} is the wave cycle rate encountered by the ship moving into the waves at speed u and is found from the theoretical (from wave spectrum) wave cycle rate ν as:

$$\omega_{\text{enc}} = \omega + \omega^2 u/g \ ; \qquad \omega = 2\pi\nu \tag{1.18}$$

where $\nu_{\text{enc}} = \omega_{\text{enc}}/2\pi$ and g is the gravitational constant. For our example, $\nu =$ 0.128Hz for the example JONSWAP spectrum used and u =5.144m/s, thus $\nu_{\text{enc}} =$ 0.182Hz.

We will first consider whether we need side waves to "better" predict fatigue damage. We will investigate this by first predicting damage from sinusoidal waves without constructing side waves. For each of the 30 waves shown in Fig. 1.10, we construct a regular sinusoidal wave for each H–T value and step the ship through this one wave cycle to get a corresponding ship load (or stress) cycle. From this one load cycle, we pick the sag bending moment as the largest positive bending moment in the cycle. Similarly, the hog moment is the largest negative bending moment in the cycle. From the 30 sag or hog moments we can then use Eqn. 1.17 to find the predicted damage. Fig. 1.12 compares predicted damage for the selected set of 30 waves **without** side waves.

The sag damage seems to be underpredicted by about 25% at $b = 1$, 70% at $b = 4$, and by about 90% at $b = 10$. Note, however, that this prediction is better than the linear sag damage shown in Fig. 1.5. Recall the linear model underpredicted damage by about 90% for $b = 4$ and by almost 2 orders of magnitude at $b = 10$. The predicted hog damage from the sinusoidal waves seems to be in good agreement over the range of b values shown. If, instead of the single-cycle bending moments, we look at the "steady-state" predicted bending moment for each of these sinusoidal

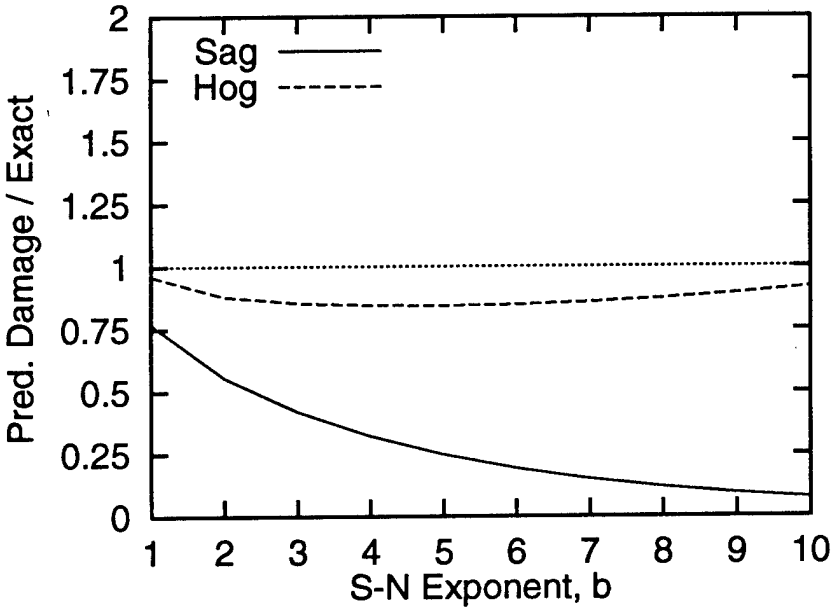

Figure 1.12: Damage prediction from response to selected sinusoidal waves. The single-wave cycle responses are used in this prediction.

waves, we find some improvement in the predicted sag damage (see Fig. 1.13). By the steady-state moment, we mean the peak response of the ship after several cycles of the same wave so that the any transient effects will have stabilized. In this case, the model underpredicts sag damage by about 10% at $b = 1$ and by about 30% at $b = 4$. Note that for large b values the steady-state damage is now overpredicted (for example, by about 50% at $b = 10$). The hog damage is still in good agreement with simulated damage.

If we predict damage based on the 30 waves, now **with** side waves (see Fig. 1.10), we find the predicted sag damage to be in good agreement with the simulated sag damage (see Fig. 1.14). This prediction seems to be very close to the exact damage, when compared with linear predicted damage in Fig. 1.5. The hog damage, however,

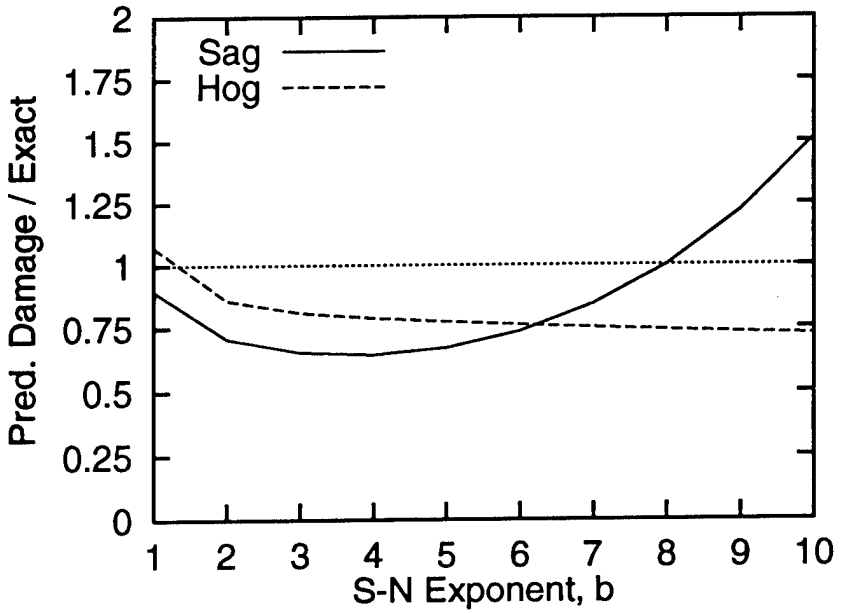

Figure 1.13: Damage prediction from response to selected sinusoidal waves. The steady-state responses to each of the regular sinusoidal waves are used in the prediction.

seems to be overpredicted for small b's by about 30% and underpredicted for large b's by about 20%.

Finally, if we choose to use only 15 waves instead of 30, the resulting sag and hog fatigue damage agreement (see Fig. 1.15) with simulated data reduces for large b's. In this case, we choose 5 different wave heights based now on a transformation of Gauss-Laguerre quadrature points and for every wave height we choose 3 wave periods based on Gauss-Hermite quadrature points [35]. The resulting choices of the wave parameters are shown in Fig. 1.16. In quadrature point selection, the main idea is to transform N standard normal or exponential random variables that have been selected to give $2N-1$ moments exactly. Standard library routines can be used to

find these quadrature points which can then be transformed using Eqns. 1.14 or 1.15 at corresponding fractiles of the random variables.

To summarize, we considered four different prediction models above: (1) single-cycle regular wave model, (2) steady-state response due to regular wave, (3) single-triplet response due to 30 regular waves with side waves, and (4) single-triplet response due to 15 regular waves with side waves. We find that each of these four models predict at least the sag damage better than a linear model. The steady-state response offers an improvement over the single-cycle regular wave model. The predictions improves further on including side waves and stepping the ship through single-triplet for each selected H–T pair. Finally, the agreement with simulated damage degrades slightly when reducing the number of waves from 15 to 30. Note that estimation of stresses and the resulting fatigue damage in each of the four models took only about 10 to 15 minutes of computer time on a HP 9000 workstation, while generation of 20 hours of simulated stresses from the random waves took about 6 days on the same computer.

In the subsequent studies, we will consider model 3 (single-triplet prediction with 30 H, T pairs) to be the base case model and attempt to further improve the agreement with simulated exact damage.

We should recognize, however, that the level of agreement seen in any of the prediction models may be due to offsetting errors. For example, the model could be predicting too large bending moments from the limited wave runs, however, the absence of any scatter effects in the model could be causing a reduction in the resulting predicted damage from the too-large bending moments. By an absence of scatter effects, we mean using only a single stress value to represent several stresses, generally random in nature, in each H–T cell (see Sec. 1.6.2).

In order to diagnose these effects, we should first compare the predicted bending

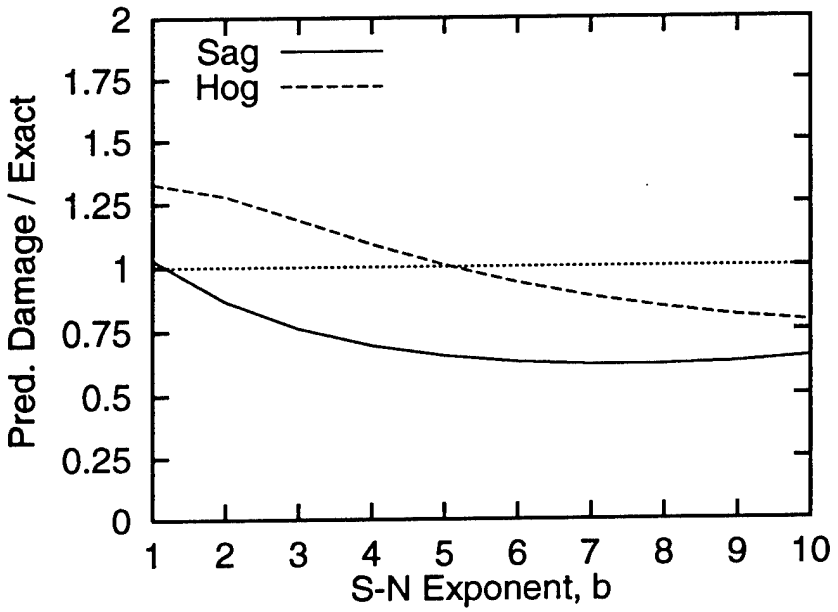

Figure 1.14: Damage prediction from response to selected waves with side waves. 30 wave triplets have been used in the fatigue prediction.

moments directly to the simulated bending moments. Any mismatch at the bending moment level should be corrected for, and then the scatter effects should be included to find fatigue damage. Another effect to be accounted for is the difference in the periods of the input wave cycle and resulting ship load cycle. We will look at the following effects in sequence to diagnose their impact on fatigue prediction:

- **Inclusion of cycle duration correction** (Sec. 1.6.1): Typically, in an irregular history of a given duration the number of wave cycles and the number of ship load cycles are different because the time domain analysis is not a static analysis. Prediction of damage per **load** cycle from damage per **wave** cycle thus may require a modification factor accounting for the duration difference that may exist between a load cycle and a wave cycle.

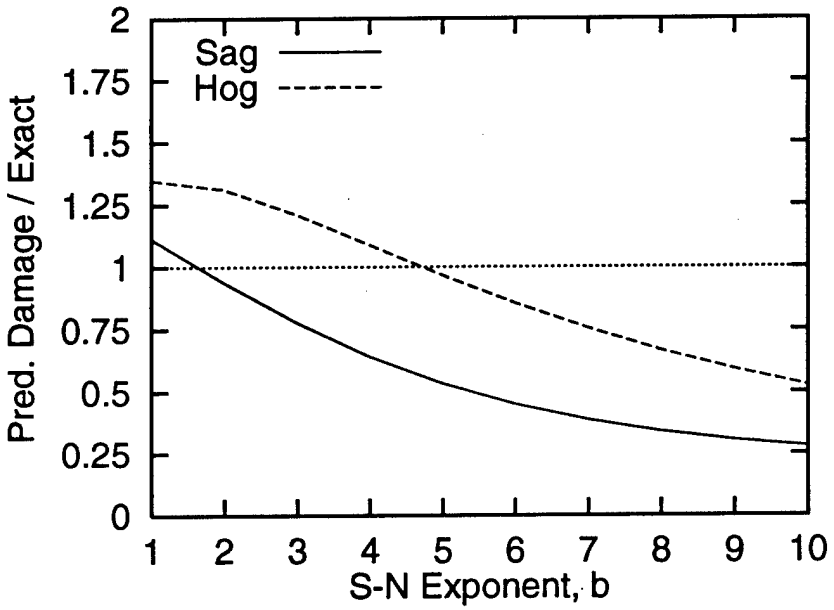

Figure 1.15: Damage prediction from response to selected waves with side waves. 15 wave triplets have been used in the fatigue prediction.

- **Inclusion of scatter effects in limited wave prediction** (Sec. 1.6.2): In the NTF model, the idea is to consider only a limited, discretized set of wave height-period pairs, $(H,T)_i$, and calculate the stress $S_i = S(H,T)_i$ associated with each. The mean value $E[S^b]$ – which is proportional to the mean damage – is then estimated from the NTF model as

$$E[S^b]_{NTF} = \sum_i p_i S(H,T)_i^b \tag{1.19}$$

Here p_i is the probability of falling into the i-th $(H-T)$ cell, centered at $(H,T)_i$. Assuming this probability p_i is correct, the "true" value of $E[S^b]$ under

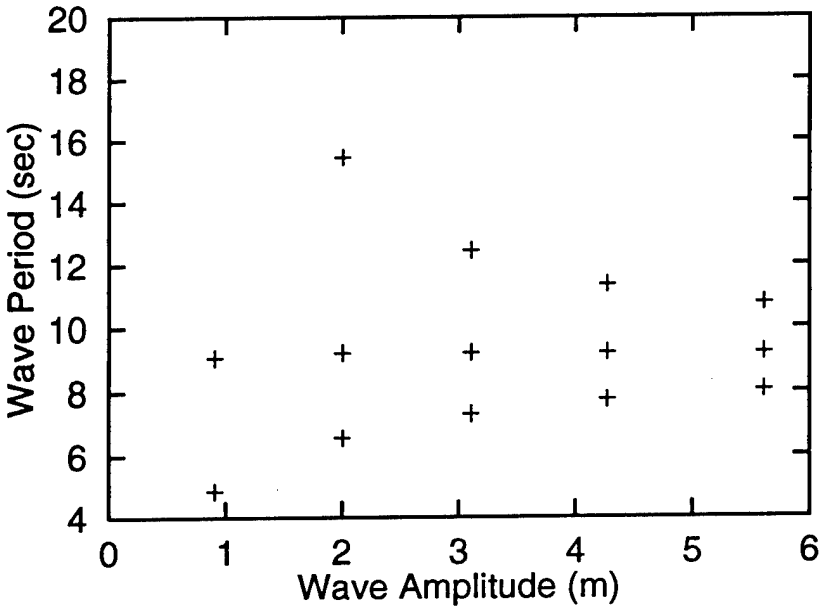

Figure 1.16: Wave parameters of the 15 waves used for predicting ship response. The wave heights and wave periods have been obtained using quadrature points. (Note the largest wave period for the smallest wave height has not been shown in this plot, to facilitate direct comparison of these parameters to the ones in Fig. 1.11)

the nonlinear simulations is

$$E[S^b] = \sum_i p_i E[S^b|H,T] \tag{1.20}$$

Thus, the critical assumption of the NTF model is quasi-static behavior, so that a wave with height H and period T always produces the same stress S=$S(H,T)$, irrespective of the past wave/stress history. In this case, because S is deterministic given H and T, $E[S^b|H,T]$=$S(H,T)_i^b$ and the NTF result becomes exact. Deviations from quasi-static behavior will produce a scatter among values of S given the same H and T, and hence $E[S^b|H,T]$ will generally exceed $S(H,T)_i^b$

(at least for $b > 1$). This effect will generally be a function of both the ship and the seastate; it will be studied here for the particular ship and seastate under consideration.

- **Inclusion of bias correction** (Sec. 1.6.3): Although we attempt to get unbiased load predictions from limited wave runs, we may have a bias in our model predictions, i.e., on average the predicted stress from a wave triplet may be too large or too small compared to a mean simulated stress corresponding to such waves from irregular waves. Any such biased estimates could be due to the inherent limitation of load prediction from short wave segments [30]. We may seek to correct for any such bias before we predict fatigue damage.

1.6.1 Modeling Duration Correction Effects

The mean damage rate based on ship load cycles is $\nu_l \overline{D_l} \propto \nu_l E[S^b]$, in which D_l is the mean damage per **load** cycle and ν_l is the load cycle rate. The mean damage rate in the NTF model is based on the wave cycles, since we estimate a single stress (sag, hog, or range) for a selected wave height and period. The mean damage rate from the NTF model then is $\nu_w \overline{D_w} \propto \nu_w E[S^b]$, in which D_w is the mean damage per **wave** cycle and ν_w is wave cycle rate. Since the actual damage per unit time occurring on the ship is the same, whether based on load cycles or on wave cycles, we should have $\nu_l \overline{D_l} = \nu_r \overline{D_w}$. In the NTF model, we base damage estimates on the theoretical wave cycles encountered, so $E[S^b]$, which yields damage per **load cycle**, should be corrected appropriately to account for the duration difference between a load cycle and a wave cycle. Thus, we could say

$$D_w = \frac{\nu_l}{\nu_w} D_l \; ; \quad \text{or} \qquad D_w = \frac{T_{\text{wave}}}{T_{\text{load}}} D_l \tag{1.21}$$

in which T_{wave} and T_{load} are the periods of a wave and the corresponding ship load cycle, respectively. Thus, the total damage based on wave cycles (from Eqn.s 1.17 and 1.21) is

$$D_P = \sum_{j=1}^{N_p} n_j S_j^b \frac{T_{\text{wave},j}}{T_{\text{load},j}} \;\; ; \;\; n_j = \text{no. of wave cycles in cell } j \tag{1.22}$$

where $T_{\text{wave},j}/T_{\text{load},j}$ is the duration correction for the jth wave and predicted load cycles.

In this study, we find when converting the damage per wave cycle to damage per load cycle, the impact of this correction on the damage estimate seems insignificant as Fig. 1.17 demonstrates. Notice how the inclusion of the duration correction makes practically no difference in the prediction in either the sag or the hog damage. An explanation for this may be that the damage-contributing loads have the load cycle periods very close to the underlying wave cycle periods, the analysis being quasi-static. We therefore propose not to include this correction in the subsequent results.

1.6.2 Modeling Scatter Effects in Ship Loads

For the waves shown in Fig. 1.11, each "+" denotes a wave pair and is considered to represent the mid-wave values of the wave parameters for the cell around it. We, then, represent the entire H-T domain by 30 cells (in this example), each of which is represented by the mid-cell H-T pair. We empirically model the scatter effects from the simulated load history by binning the 20 hours load history in this H-T space and modeling the resulting load scatter in each cell. In each load cycle, we identify the loads as, (1) sag: the maximum (positive) load in the cycle, (2) hog: the minimum

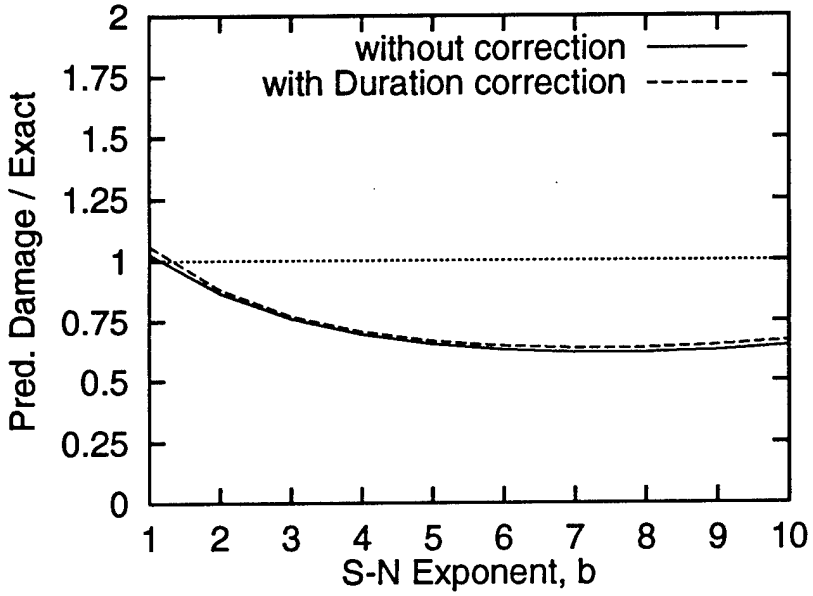

(a) Sag Fatigue Damage

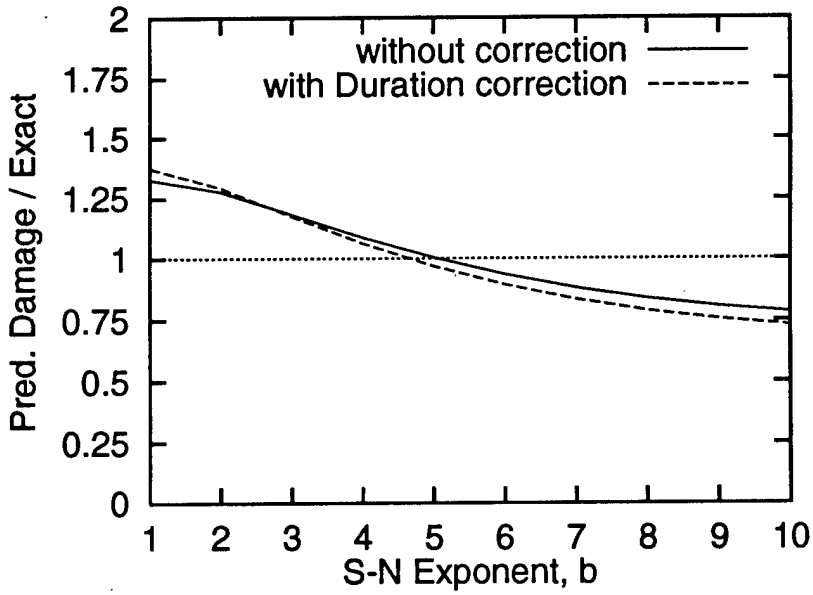

(b) Hog Fatigue Damage

Figure 1.17: Demonstration of impact of duration correction on predicted fatigue damage for sag and hog bending moments

(negative) load in the cycle, and (3) range (=sag+hog). The 2-dimensional binning of each of the ship loads is then based on the H-T of the wave cycle causing this load cycle.

The mean μ and standard deviation σ of the binned loads in every cell results in a coefficient of variation COV $= \sigma/\mu$ of the ship loads. A straight line fit to this simulated COV vs. wave heights is referred to, in this study, as the empirical COV (see Figures 1.18 and 1.19). Here T_1, T_2, T_3 refer to the 84, 50 and 16 percentile conditional periods given the wave heights (see Fig. 1.11 for actual values of these periods). In general, the COV values in the cells may depend on the bin size. In this study, however, we find that making the 2D bins 4 times smaller or make it 2 times as coarse, still results in about the same COV values, suggesting that COV dependence on bin size seems to be insensitive to a broad range of bin sizes.

In order to understand the impact of scatter effects on fatigue damage prediction, we bin the simulated bending moments according to the chosen 30 pairs of wave parameters, and then compare the exact simulated damage to that estimated only from the mean simulated loads $\overline{S}$ in the bins as done in the prediction models. The simulated damage without including scatter effects gives the total damage as

$$D_t = \sum_{j=1}^{N_p} n_j \left(\overline{S}\right)_j^b \quad ; \quad n_j = \text{number of load cycles in cell } j \tag{1.23}$$

Figure 1.20 shows a ratio of total damage from this model (Eqn. 1.23) to the exact damage (Eqn. 1.9).

As seen, Eqn. 1.23 (damage without scatter effects) will underpredict the fatigue damage by as much as 25% for steel materials ($b = 4$) and by about 60% for composite materials ($b = 10$). Because of nonlinear effects, the hog loads are typically smaller than the sag loads (see Fig. 1.4), and so if scatter effects are ignored, the hog damage

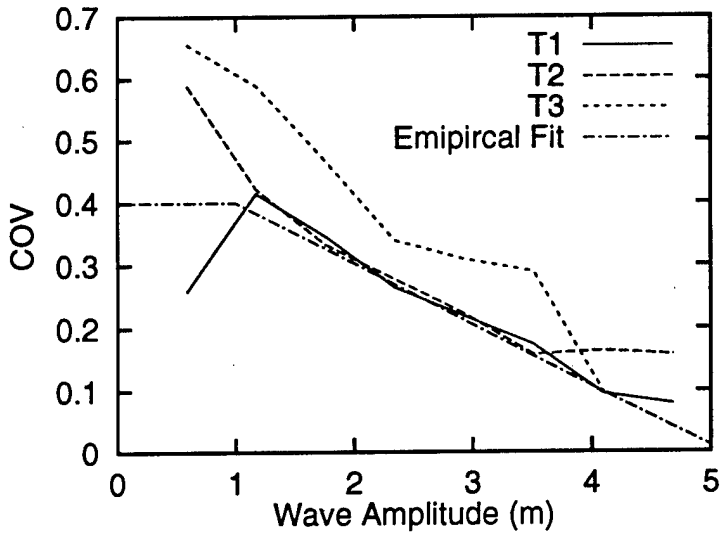

(a) Sag Load

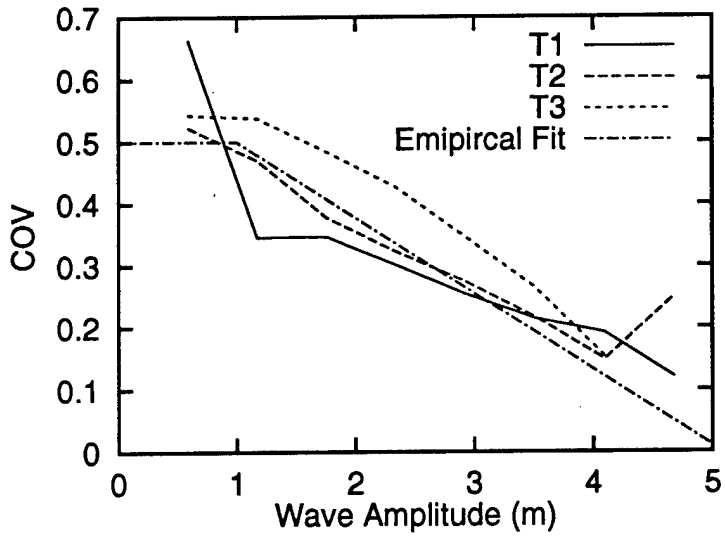

(b) Hog Load

Figure 1.18: Coefficient of Variation (COV) of simulated ship loads (sag and hog) for H–T cells in Fig. 1.11

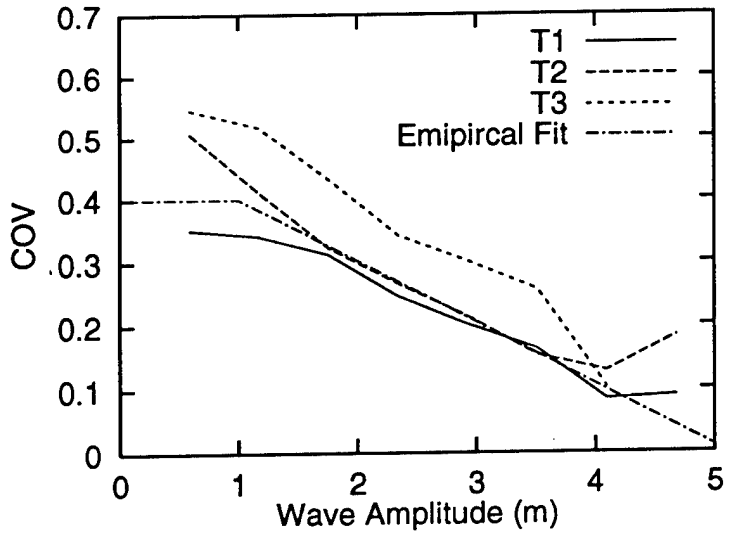

Figure 1.19: Coefficient of Variation (COV) of simulated ship loads (range) for H–T cells in Fig. 1.11

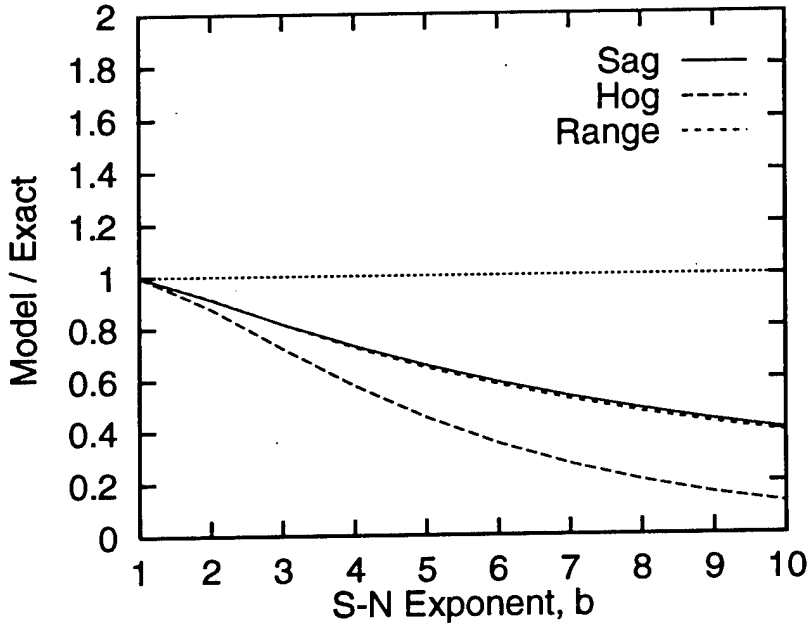

Figure 1.20: Demonstration of need for scatter estimate of response in H–T cells

is affected more than sag; also the range (= sag + hog) dominated by sag contribution is influenced by the scatter effects in a manner similar to the sag load. As a simple example, the extent to which scatter effects matter can be seen when estimating $E[S^2]$ from $\overline{S}$:

$$E[S^2] = \text{Var}[S] + \overline{S}^2 = \overline{S}^2 \left(1 + \text{COV}^2\right) \tag{1.24}$$

where $\text{Var}[S]$ denotes the variance of S. A factor $1 + \text{COV}^2$ larger than 1 is needed to inflate $\overline{S}^2$ to find $E[S^2]$ exactly; similarly, still larger factors will be required to estimate $E[S^b]$ from $\overline{S}^b$ for $b > 2$. As demonstrated in the following sections, we strive to predict exact $E[S^b]$ from a Weibull model calibrated only to the first two moments of S.

In order to include scatter effects in the predicted damage, we use the NTF predicted bending moment in a cell and the empirical COV in that cell to calibrate a Weibull model for the load in that cell. For a Weibull load (S) model with shape parameter α and scale parameter β, the exceedance probability is $P[S > s] = \exp[-(s/\beta)^\alpha]$, where α and β are tuned to the NTF predicted bending moment and the COV in each cell. Fatigue damage, proportional to $E[S^b]$, is then found from this fitted Weibull model as $E[S^b] = \beta^b \Gamma(1 + b/\alpha)$. A weighted sum of this $E[S^b]$ across all the cells results in the total predicted fatigue damage.

Fig. 1.21 shows the predicted damage from the 30 wave triplets, including the empirical COV estimate, compared to exact damage for sag and hog bending moments. Inclusion of scatter effects for sag damage prediction, further improves the damage prediction. Now the predicted sag damage is within 10% error for all b's shown in the plot. Again, compare this with the linear damage estimate in Fig. 1.5 that considerably underpredicts the sag damage. The hog damage, on the other hand, seems to be on the conservative side at all b values, on including the scatter effects. Note,

however, that at $b = 1$ the hog damage is overpredicted by about 35%, implying that this may be a case where triplet-wave hog moment prediction is biased towards too large hog moments. We will investigate this in the next section, where we will compare the predicted moments to the mean simulated moment in each cell.

1.6.3 Inclusion of Bias Correction in the Prediction Model

To compare predicted bending moments to the simulated bending moments, we bin the 20 hours of nonlinear bending moments according to the 30 H, T pairs (shown in Fig. 1.11). Figures 1.22 and 1.23 show a comparison of the mean simulated bending moments to the predicted bending moments in each H, T cell as a function of $a = H/2$. In this figure, T1, T2, and T3 refer to the 16-, 50- and 84- percentile period values at the given H value (see Fig. 1.11 for actual values of the three periods given H). The predicted sag bending moment compares closely to the simulated sag moment, on average. This observation is in agreement with the close comparison we find for sag damage prediction at $b = 1$ in Fig. 1.21a. The hog bending moment is systematically overpredicted by approximately 20% and, consequently, the range bending moment is overpredicted by about 10%. These overpredictions may be due to an intrinsic limitation of the model in predicting hog moments from wave triplets. In any case, these overprediction factors can be treated as bias corrections to the predicted bending moments when estimating fatigue damage. As a result the predicted hog bending moments should be reduced by a factor of about 0.85 ($\approx$ 1/1.20) and the range bending moment by a factor = 0.92 ($\approx$ 1/1.0). The bias correction factors may also be found from Fig. 1.17b, where the model overpredicts the hog damage by approximately a factor of 1.35. Consequently the range (=sag+hog) moment will be overpredicted by a factor of about 1.175 [= (1+1.35)/2]. No bias correction will be

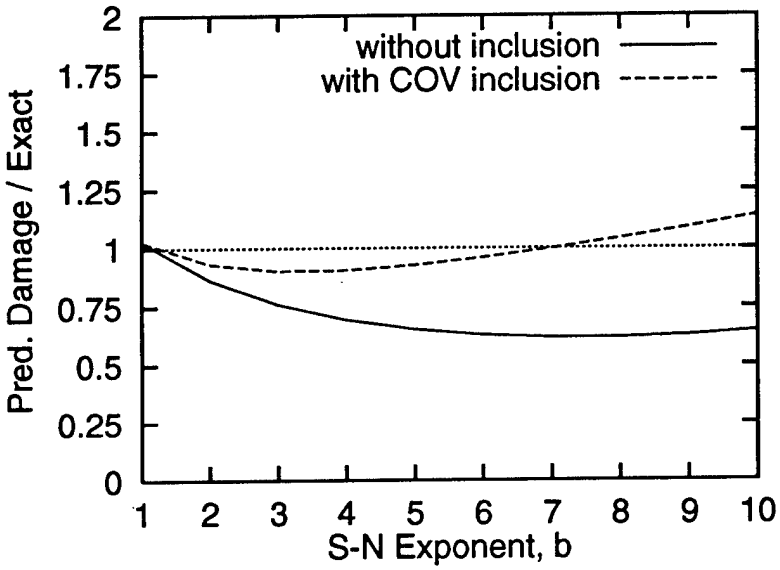

(a) Sag Fatigue Damage

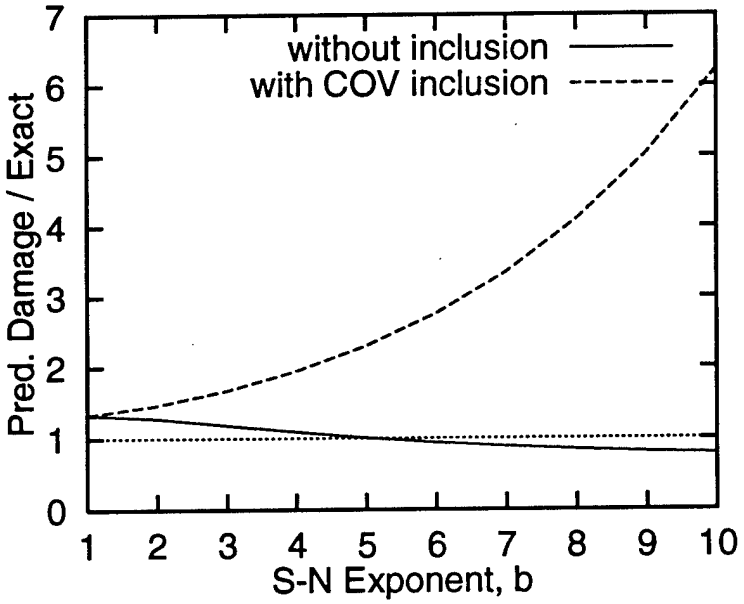

(b) Hog Fatigue Damage

Figure 1.21: Demonstration of impact of inclusion of scatter effects in the predicted fatigue damage for sag and hog bending moments

applied to the sag bending moment damage prediction. We will now investigate the impact of these bias-corrections on fatigue damage.

Fig. 1.24 compares the predicted hog damage, with and without any bias correction, to exact damage. Note that all the hog damage predictions here include the scatter effects. As a result, the bias-corrected prediction is now from Weibull stress models in each cell, where α and β have been tuned to the bias-corrected hog bending moment and to the empirical COV from Figs. 1.18 and 1.19. Note how good the agreement in the predicted and exact damage is, when including the bias factor of 0.85. When a reduction factor of 0.75 is used, the first moment $E[S]$, of course, matches the exact value, however, damage for $b > 1$ seems consistently underpredicted. Further investigation on an optimum choice of the bias factor has not been done in this study. Realize, however, that in order to calibrate any bias-correction factor, a limited nonlinear analysis will have to be performed on irregular waves, as similarly required in obtaining the COV corrections.

Finally, we present a comparison of the NTF predicted damage together with the linear damage results compared to the nonlinear exact damage on the same plot. This is to directly study the difference in results. Note that no new results are being shown here, though. The NTF prediction includes bias-corrections for hog (factor=0.85) and range (factor=0.92) bending moments and includes the scatter effects for all three: sag, hog and range bending moments. Figures 1.25 and 1.26 show a comparison of total fatigue damage in 20 hours in this example seastate from the NTF model and from linear theory compared to simulated total nonlinear fatigue damage for a range of S-N exponents. Recall the significance of this example seastate is that according to linear theory it contributes most to the long-term fatigue damage (see Fig. 1.6) for an S-N exponent of 4. As seen in Fig. 1.25a, linear theory

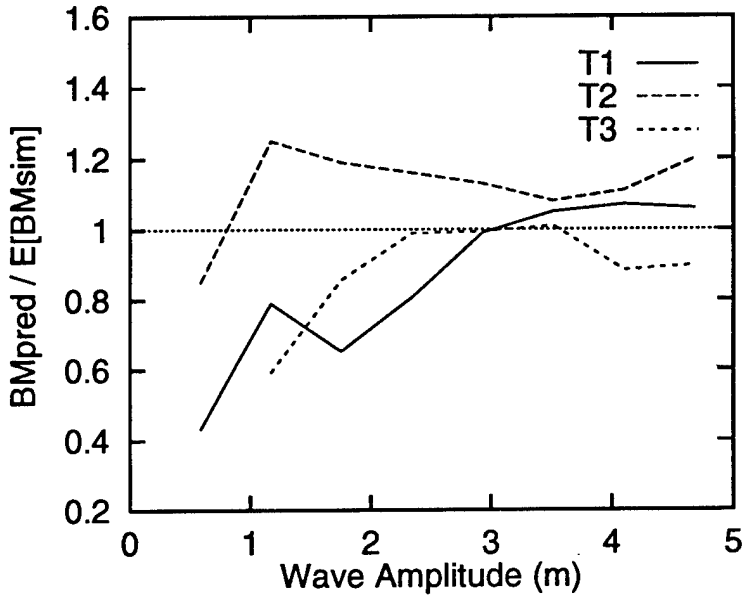

(a) Sag Load

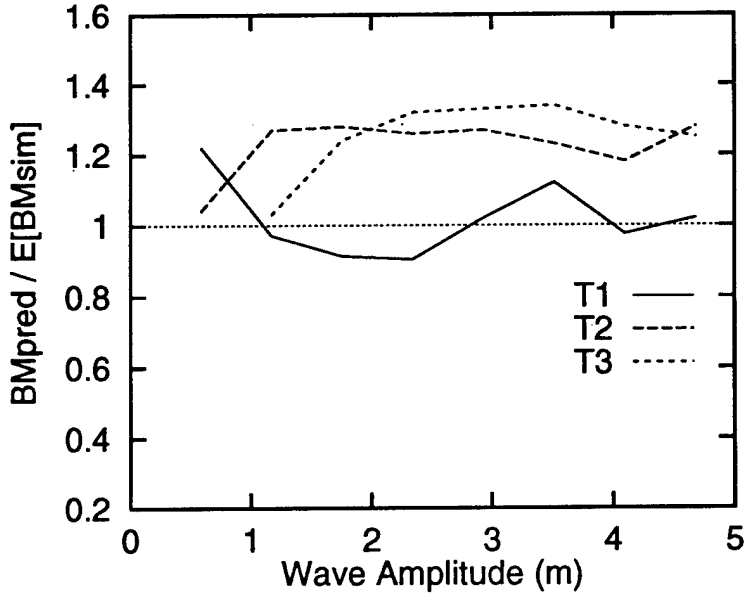

(b) Hog Load

Figure 1.22: Ratios of predicted to mean simulated (sag and hog) bending moments in H–T cells

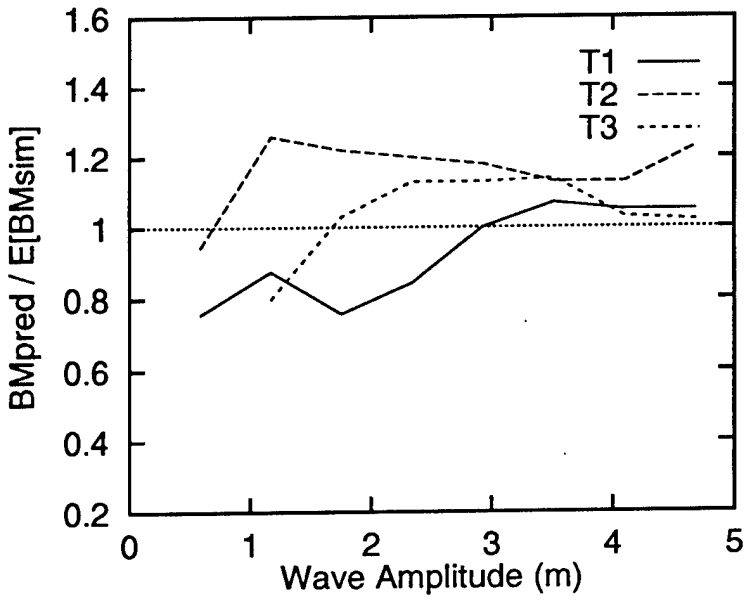

Figure 1.23: Ratios of predicted to mean simulated (range) bending moments in H–T cells

considerably underpredicts fatigue damage for sag bending moments, while the NTF model offers excellent prediction over the entire range of S-N exponents. For hog fatigue damage, the NTF prediction is much closer to simulation than is linear theory. For range bending moments, considered in damage prediction using Miner's rule, we see that linear theory underpredicts damage while the NTF prediction is very close to simulation.

In summary, linear theory considerably underpredicts sag and range loads and damages, while the NTF model offers excellent agreement with the nonlinear loads and damages.

Note that the 20 hours of nonlinear irregular wave simulation used in this study took about 160 hours ($\approx$ 6.5 days) of total computer time, while the NTF model without the COV or bias correction took only about 10 minutes of computer time.

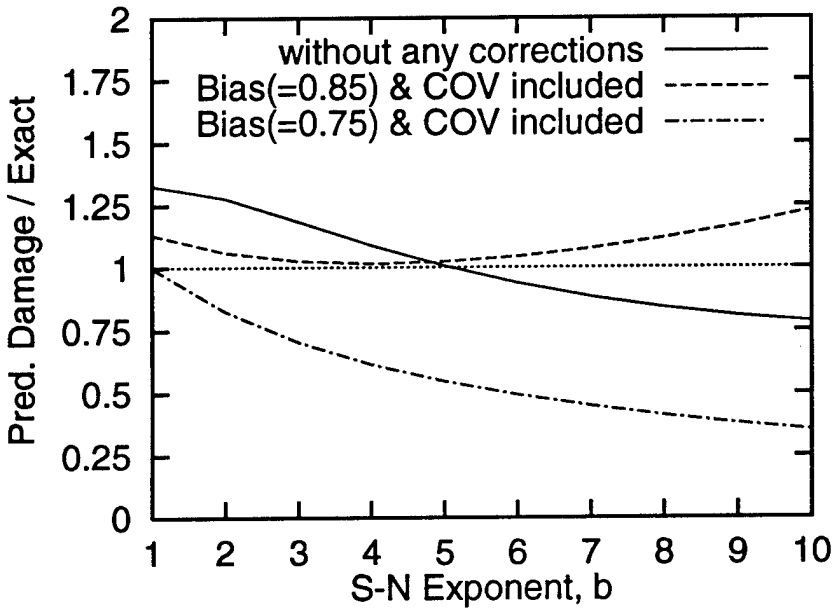

Figure 1.24: Effects of including bias-correction in hog damage prediction

While the complete nonlinear analysis is only a 2-D analysis, a 3-D analysis of the nonlinear responses is predicted to take about 10 to 20 times longer than the 2-D analysis. In conclusion, the NTF model appears to offer an economical alternative to complete nonlinear time domain analysis for estimating fatigue damage.

1.7 Conclusions and Future Work

1.7.1 Conclusions

In this study, we propose a "Nonlinear Transfer Function" model for estimating fatigue damage from a limited set of sinusoidal waves and their associated probabilities from stochastic process theory. A simple version of the NTF model, where for each

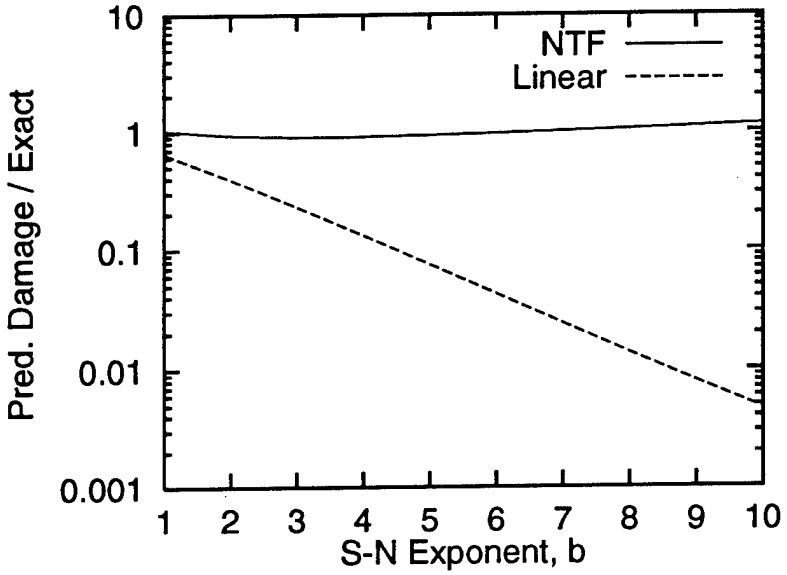

(a) Sag Fatigue Damage

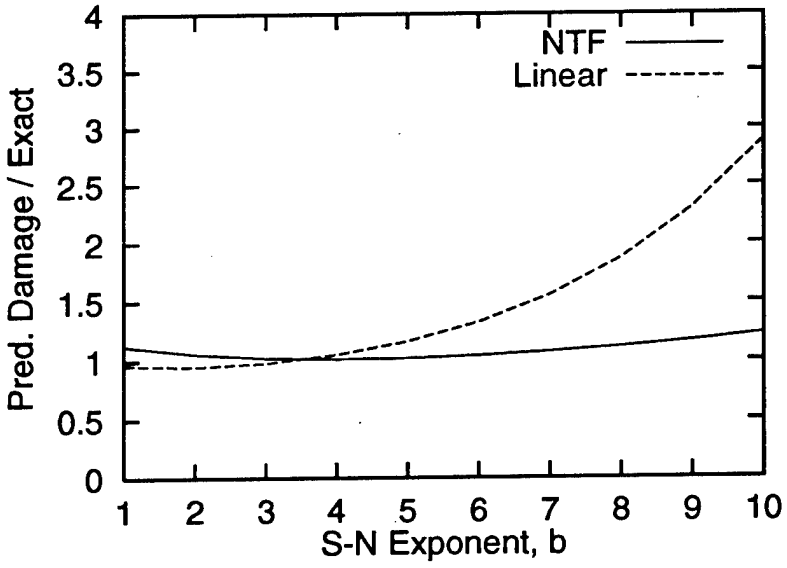

(b) Hog Fatigue Damage

Figure 1.25: Linear, NTF, and Nonlinear Bending Moment Fatigue Damage for Range of S-N Exponents

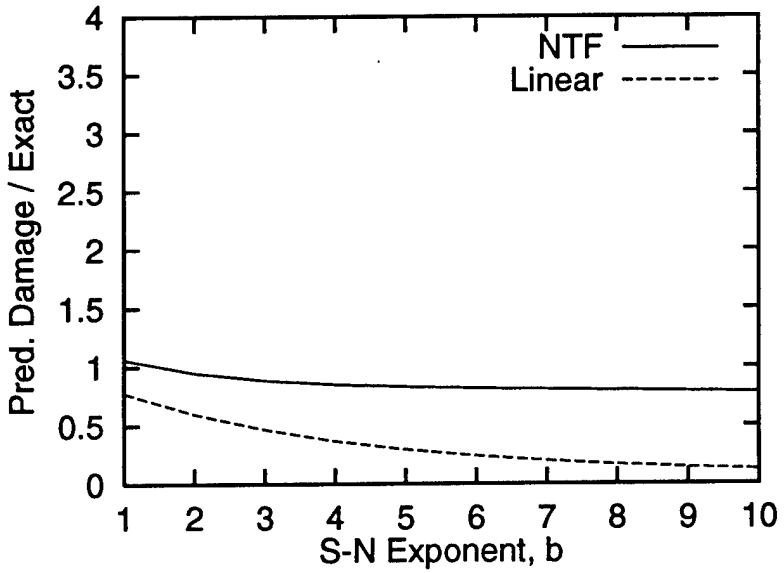

Figure 1.26: Linear, NTF, and Nonlinear Bending Moment (Ranges) Fatigue Damage for Range of S-N Exponents

selected wave height and wave period we construct side waves and apply the wave triplet on to the ship. The resulting set of stress (sag, hog, and range) for selected set of waves, along the theoretical probabilities of seeing the waves can be used to find predicted fatigue damage estimates. This damage estimate agrees well with that estimated from a complete random wave analysis, which is general is an expensive calculation. A linear analysis, on the other hand, appears to severely underpredict the sag-induced damage, while the hog damage seems to compare with the nonlinear time domain analysis in random waves. Note the NTF predicted damage took on the order of minutes of computer time, while the random wave analysis studied here took about 8 hours of computer to simulate 1 hour of stress time histories.

The agreement in the NTF prediction can be improved further by accounting scatter effects in the observed stresses. The hog damage estimation appeared to

require a bias correction in addition. We propose use of short duration simulations in random waves in order to estimate the scatter effects and to estimate the bias factors for hog and range stresses. This still alleviates the need for long simulations to find exact fatigue damage estimates. For this flared ship in ship-length tuned seastate considered, we find the current state-of-the-art spectral analysis methods to yield considerably unconservative sag fatigue damage, and overpredict hog fatigue damage, and find that the NTF model offers a cheaper alternative and yields a more precise estimate of fatigue damage when compared to that from nonlinear time domain analysis in random waves.

Further studies should be done to investigate generalities of this model: across different ship models, across different seastates. We speculate that the NTF model (single-triplet predictions) should be able to successfully predict damage in other seastates as well, since the seastate chosen here was supposed to severely test the model.

1.7.2 Future Work

The NTF predictions were compared to the nonlinear analysis results in a single seastate. We suggest additional comparisons be performed in other seastates as well; and finally compare the long-term predicted damage from the NTF model to simulated long-term damage from the nonlinear analysis. The nonlinear analysis could be performed across a set of climate conditions (H_s, T_p) with probabilities chosen to reflect the long-term distribution of these parameters. The simulated damage in each of these seastates could be weighted and summed to result in a long-term damage from the nonlinear analysis. The NTF model, on the other hand, may be used to predict fatigue from a selected set of wave heights and wave periods whose occurrence

probabilities reflect the long-term distribution of the wave parameters. The nonlinear stresses from these selected waves can then be used to predict the long-term NTF fatigue damage. An agreement in these two long-term damage estimate will further test the NTF model capabilities. We could similarly predict and compare long-term fatigue damage from a linear analysis as well to demonstrate performance of linear analysis in predicting long-term fatigue damage.

As part of the future work, we also recommend that the NTF model studies be generalized to other seastates, other loads on the ship, other ship models, and to other ship analysis programs. Finally, impact of nonlinearities in the waves on fatigue in ship can be investigated by analyzing the ship in waves simulated from the second-order wave model, instead of using linear (Gaussian) waves.

Chapter 2

Ship Fatigue Reliability

2.1 Introduction

This chapter describes a fatigue reliability analysis for the ship structure considered in Chapter 1. A general methodology for fatigue analysis is presented and numerical results are shown for a specific application to ship structures. The methodology presented here is largely adapted from Reference [17].

2.2 General Fatigue Formulation

The assumption is that a complete reliability formulation generally includes uncertainly in three distinct aspects:

1. The loading environment, characterized here by random variables;

2. The gross level of structural response, given the load environment; and

3. The local failure criterion, given both the load and the gross stress response.

The general fatigue formulation requires three functional inputs: $f_{X_1}(x_1)$, $f_{S|X_1}(s|x_1)$ and $N_f(s)$ to characterize the load, response and fatigue damage, respectively. Here $f_{X_1}(x_1)$ is probability density of the environment variable X_1, $f_{S|X_1}(s|x_1)$ is conditional probability density of the gross stress S given X_1 and $N_f(s)$ is the number of constant stress cycles with amplitude s after which the component fails. The mean damage rate $\overline{D}$ is found by integrating over all load and response levels x_1 and s:

$$\overline{D} = \int_{x_1=0}^{\infty} \int_{s=0}^{\infty} \frac{f_{S|X_1}(s|x_1) f_{X_1}(x_1)}{N_f(s)} ds\, dx_1 \tag{2.1}$$

If failure is defined when damage reaches a threshold Δ, we have the time to fail

$$T_f = \Delta/(f_0 \overline{D}) \tag{2.2}$$

where f_0 is the stress cycle rate. If Miner's rule is correct we would assign $\Delta = 1$. More generally, variability in Δ would reflect the uncertainty in Miner's rule, i.e., the effect of predicting variable-amplitude fatigue behavior from constant-amplitude tests.

For the reliability analysis, the failure criterion is taken to be the difference between the computed fatigue life T_f in Eqn. 2.2 and a specified target lifetime, T_t.

$$G(X) = T_f - T_t \tag{2.3}$$

$G(X)$ is known as the failure state function that depends on all the associated random variables X. $G(X)$ is positive when the component is safe and negative when it has failed. First-order reliability methods (FORM) [24] can be used to find the failure probability, $P_f = \text{Prob.}[G(X) < 0]$.

We examine each of these in turn below for an offshore structure.

2.2.1 Load Environment

We assume that the long-term environment can be characterized by one environment variable X_1. This could be H_s, the significant wave height describing the short-term climate conditions. A distribution of X_1 should be chosen to describe the long-term variation of the climate along the ship route (e.g., [8]). In this study, we choose the wave heights H, instead, as the environment variable X_1, and describe it by a long-term Weibull distribution. Note that H is a local wave height that is the distance from the minimum elevation to the maximum elevation in wave cycle. Here, a wave cycle is the wave surface between two mean upcrossings.

In a short-term seastate with given H_s (typically lasting 1 to 6 hours), we assume H to be Forristall distributed (see Reference [15]). Note that in the ship fatigue analysis studies (Chapter 1), we had found that the Forristall model well predicted the simulated wave heights. This short-term distribution is given as

$$\text{Prob.}[H > h] = \exp\left[-\frac{(h/\sigma_\eta)^{2.126}}{8.42}\right] \tag{2.4}$$

in which $\sigma_\eta = H_s/4$. The long-term distribution $f_{LT}(h_{LT})$ of the wave heights can be found from the short-term Forristall distribution $f_{ST}(h|H_s)$ given H_s as

$$f_{LT}(h_{LT}) = \int_{h_s=0}^{\infty} f_{ST}(h|H_s) f_{H_s}(h_s)\, dh_s \tag{2.5}$$

in which $f_{H_s}(h_s)$ is the long-term distribution of H_s. To demonstrate the methodology in this study, we arbitrarily assume H_s to have a Weibull distribution with mean $E[H_s] = 3$ meters and variance $\text{Var}[H_s] = 3.6$ m^2 [24]. $f_{LT}(h_{LT})$ in Eqn. 2.5 above,

is approximated to be a two-parameter distribution type. The two parameters are calibrated to the first two moments $E[H_{LT}]$ and $E[H_{LT}^2]$ of the long-term wave heights. These moments can readily be found from the conditional distribution as

$$E[H_{LT}] = E_{H_s}[E[H|H_s]]\ ; \quad E[H_{LT}^2] = E_{H_s}[E[H^2|H_s]] \tag{2.6}$$

where $E_{H_s}[]$ indicates taking expectation of random variable H_s. From these calculations we find the mean and the coefficient of variation (COV) of the long-term wave heights to be:

$$E[H_{LT}] = 1.81\text{meters} \qquad \text{COV}[H_{LT}] = 0.857$$

2.2.2 Gross Response

The stress response at the location of interest is, in general, random in nature and dependent on the underlying environment X_1. The stress may be described by a conditional distribution $f_{S|X_1}(s|x_1)$, which is assumed to be a two-parameter distribution type in this study. The two parameters are found from the conditional mean and standard deviation of of the stress S given the environment variable X_1 denoted $S|X_1$. In this application, we assume that the stress S given X_1 has a Weibull distribution type, whose parameters can be found from the mean and standard deviation of the conditional stresses.

For this study, we select the same ship as considered in Chapter 1 and use the nonlinear time domain analysis program NV1418 [11] to find the stresses in random wave conditions. We again select the seastate described by $H_s = 5$m and $T_p = 10$s to analyze the ship response. Recall that this was the most damaging seastate according

to a linear analysis and expect to be so even according to a nonlinear analysis. The mean relation of $S|H$ found from this seastate should, generally, be applicable for all wave heights H regardless of the seastate. The wave period dependence of the stresses (ignored in this study) may, however, effect the scatter of stresses about the mean regression line; and this scatter is likely to be seastate- or T_p-dependent.

For each wave height in this one hour seastate we find the corresponding bending moments (sag, hog, and range) in the response history. A regression analysis of the form $E[S|H] = aH^p$ was performed, to fit the mean bending moment (or stress S) given H. We used a nonlinear least-squares regression method called Levenberg-Marquardt method [28] as implemented in Gnuplot [34] to estimate the mean values of the parameters a, p, their standard errors σ_a, σ_p and correlation ρ_{ap} for this data set. The standard errors reflect the uncertainty in the estimated parameters due to limited data. The regression assumed a constant conditional standard deviation $\sigma_{S|H}$, although this scatter should generally increase with increasing wave heights. In this illustration, we assume that the bending moment can be converted to stresses by simply dividing by an appropriate section modulus.

Note that the regression is based on only one seastate, the most damaging seastate. The mean regression line is assumed to be valid across all the seastates. The variability of stresses $\sigma_{S|H}$ about this mean trend, in general, may vary across different seastates. In this example, however, we will assume no uncertainty in the estimated $\sigma_{S|H}$.

As mentioned earlier, from one hour simulation of bending moments in irregular seas (H_s = 5m and T_p = 10s), we relate the wave heights to the corresponding sag, hog, and range bending moments (BM) assuming the following functional form:

$$E[\mathrm{BM}|H] = aH^p \tag{2.7}$$

Table 2.1: Estimated mean and standard deviation of the regression parameters for bending moments (kN.m) given wave heights. The bending moments have been divided by 10^5.

Moment	a	σ_a	p	σ_p	ρ_{ap}	$\sigma_{S\|H}$
Sag	0.453	0.0284	1.168	0.0404	−0.972	0.746
Hog	0.617	0.0354	0.619	0.0410	−0.945	0.593
Half-Range	0.504	0.0276	0.951	0.0366	−0.965	0.592

Figs. 2.1 and 2.2 show the resulting regression fits to the simulated bending moments. Table 2.1 gives the numerical values of the estimated parameters.

In converting the bending moments to stresses we will use a constant section modulus (= 35 m^3, here). In the subsequent reliability analysis, we will additionally multiply the stresses by 10^{-3} to convert to units of MPa (or N/mm^2) so as to consistently use the S–N data also given in MPa.

2.2.3 Failure Measure

We assume that fatigue test data are available at constant stress amplitudes to estimate the S–N curves. These curves present the number of stress cycles to fail for a given constant stress amplitude load on the fatigue specimen. We use Miner's rule to assign damage $1/N_f(s)$ due to a single stress amplitude s. The fatigue damage is then characterized by $\overline{D}$, the mean damage rate. Any variation about the mean rate will average out when accumulating damage across the high-cycle fatigue applications of interest here. As a result the fatigue damage is characterized by only the mean damage rate $\overline{D}$, and hence by only the S–N curve.

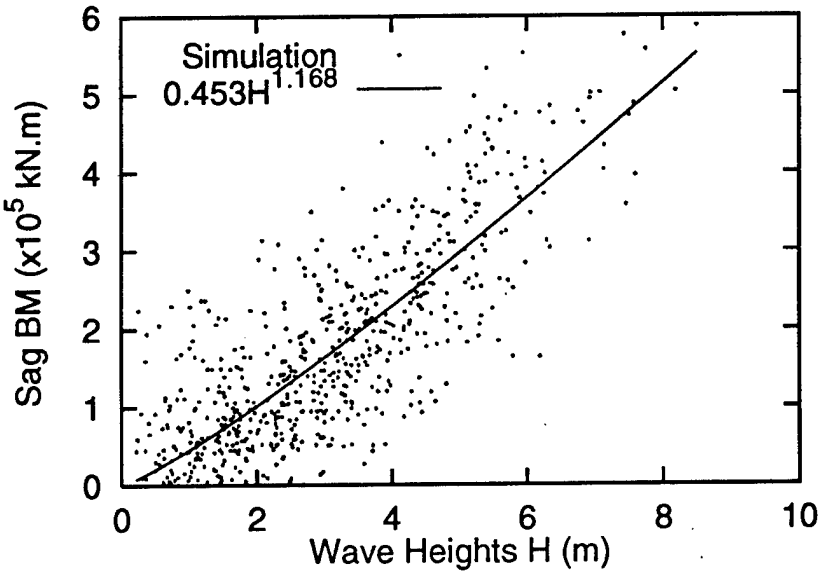

(a) Sag bending moment

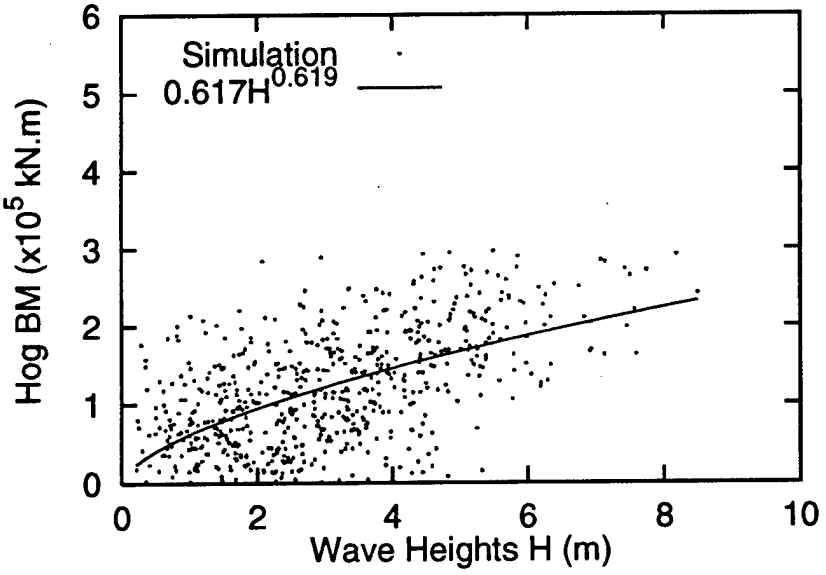

(b) Hog bending moment

Figure 2.1: Nonlinear least squares regression analysis to fit sag, and hog bending moments to wave heights from 1 hour simulation of bending moments in seastate with $H_s = 5$m, and $T_p = 10$sec.

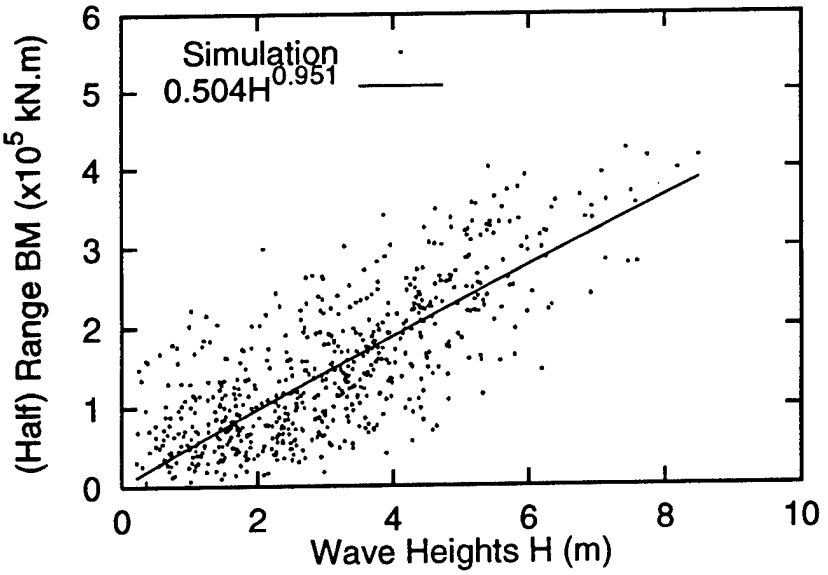

Figure 2.2: Nonlinear least squares regression analysis to fit half-range bending moments to wave heights from 1 hour simulation of bending moments in seastate with $H_s = 5$m, and $T_p = 10$sec.

As described in Chapter 1, typically the S–N curve is specified as

$$N = CS^{-b} \tag{2.8}$$

where C, b are the intercept and the slope of the fitted curve to $\log S$ to $\log N$ data. In general, both C and b are random in nature and C typically shows a large uncertainty – COV of the order of 50 to 60%. The regression relation gives the mean number of stress loading cycles N with amplitude S that a fatigue specimen can tolerate before failing [12]. Typical values of b for steel material may be 3–6, and may be as high as 7–10 for composite materials. Values of S–N parameters for offshore structure materials and their uncertainties can be found in various literature, including API [2]

and SSC reports [26] among others.

2.3 Results

2.3.1 Numerical Values for Random Variables in Fatigue Analysis

Recall that the sag stresses cause fatigue cracks at the ship bottom and the hog stresses cause fatigue cracks in the ship deck. Other approaches use the stresses due to the range bending moments to analyze the fatigue cracks at either of these locations. Of interest is the fatigue reliability of an element (here, at the ship bottom or the ship deck) in a specified lifetime. We will show that using the sag, hog or range stresses generally leads to different estimates of reliability or the probability of failure.

The input random variables in the example fatigue analysis and their values are given in Table 2.2. The random variables listed here are common to the three stress cases (sag, hog, and range) we consider here. The COV values in Table 2.2 have been arbitrarily chosen and should generally reflect the uncertainty in the parameters either due to limited data or due to lack of knowledge. The parameters relating stresses to wave heights are given in Table 2.1. To calibrate the median time to fail $\breve{T}_f$ to a desired lifetime, we introduce an additional factor δ in Eqn. 2.2 so that we have

$$T_f = \delta \frac{C\Delta}{f_0(SCF)^b} \tag{2.9}$$

In this equation, we set all the random variables to their median values and calibrate δ so that we get $\breve{T}_f = 200$. Table 2.3 gives the values for δ for each of the three cases.

Table 2.2: Numerical values of means and COVs of random variables and their distribution types used in fatigue formulation. These are common to all three stresses: sag, hog and range.

Variable	Mean	COV	Dist.Type	Description
$E[X_1]$	1.81 (m)	0.05	Normal	Mean of Long-term H
COV$[X_1]$	0.857	0.1	Normal	COV of long-term H
f_0	0.1 (Hz)	0.2	Normal	Stress cycle rate
SCF	2.5	0.1	Normal	Stress concentration factor
C	2.4×10^{15}	0.5	Weibull	S–N factor
b	4	0	–	S–N exponent
Δ	1	0.1	Normal	Damage threshold

Table 2.3: Calibrated factor δ for the three cases: sag, hog and range. Note that δ is a deterministic variable.

Variable	Sag	Hog	Range
δ	0.02084	0.003463	0.007669

Using the above random variables, we performed a FORM analysis to find the failure probabilities for a range of specified target lifetimes. In order to find the failure probabilities, all the random variables X are first transformed into a uncorrelated normal U-space. The failure state function $G(X) = 0$ is evaluated in the normal U-space and gradient search methods are employed to find the point on the failure surface closest to the origin. This is the most likely failure point and is also referred to as the design point. Approximation of the failure probability if obtained by fitting a tangent plane (first-order reliability method, FORM) or a parabolic surface (second-order reliability methods, SORM) to the failure state function at the design point. The direction cosines of the vector that defines the design point are the relative measures of the importance of each of the random variables.

Fig. 2.3 compares these failure probabilities for the three different cases. The

P_f estimates are somewhat different for the three stress cases. For a given target lifetime, the sag stress gives the largest P_f followed by range stress, and then the hog stress Even though the median time to fail is the same in all the three cases, we see such a difference because of the different conditional trends of the stresses given the wave heights that imply different magnification of the wave parameter uncertainty. Since the sag trend shows the largest nonlinearity, the wave parameter uncertainty is amplified the most among the three and this results in the largest P_f for given service lifetime. For example, at around the typical design life of 20 years, the sag case gives $P_f = 0.011$, the range case gives $P_f = 0.0093$, while the hog case gives $P_f = 0.0081$. Recall that hog stresses may cause cracks in the ship deck, while the sag stresses cause cracks in the ship bottom. The P_f comparison then implies that the element at the ship deck is about 1.4 times as likely to fail compared to the ship bottom element, even though both have $\breve{T}_f = 200$ years.

2.3.2 Importance Factors of Physical Random Variables

Table 2.4 gives the values of the random variables at the design points and their uncertainty contributions (squares of the direction cosines) for each of sag, hog and range cases.

The values of the random variables at the design point can be used to design the structural element and the FORM analysis would predict the design to yield the reliability level as indicated in Fig. 2.3 for a service life of 20 years. This table also indicates the relative importance or uncertainty contributions of the different random variables. In all the three cases, we see that the S–N factor C carries the most importance, followed by the SCF and the environment variables. The environmental variables seem to relatively more important in the sag case than in the hog case. This

Table 2.4: Values of associated random variables at "failure" point and their uncertainty contributions (for Service life of 20 years)

Sag Case		
Var.	Value	Uncert. Contrib.
$E[X_1]$	1.842	0.024
COV$[X_1]$	0.917	0.094
a	0.450	0.002
p	1.173	0.003
f_0	0.1066	0.021
SCF	2.664	0.082
C	4.495E+14	0.769
Δ	0.982	0.006

Hog Case		
Var.	Value	Uncert. Contrib.
$E[X_1]$	1.819	0.002
COV$[X_1]$	0.8669	0.002
a	0.6170	0.000
p	0.6199	0.001
f_0	0.1067	0.020
SCF	2.668	0.078
C	3.260E+14	0.891
Δ	0.9815	0.006

Half-Range Case		
Var.	Value	Uncert. Contrib.
$E[X_1]$	1.830	0.009
COV$[X_1]$	0.8965	0.038
a	0.5019	0.001
p	0.9548	0.001
f_0	0.1067	0.020
SCF	2.667	0.080
C	3.722E+14	0.844
Δ	0.982	0.006

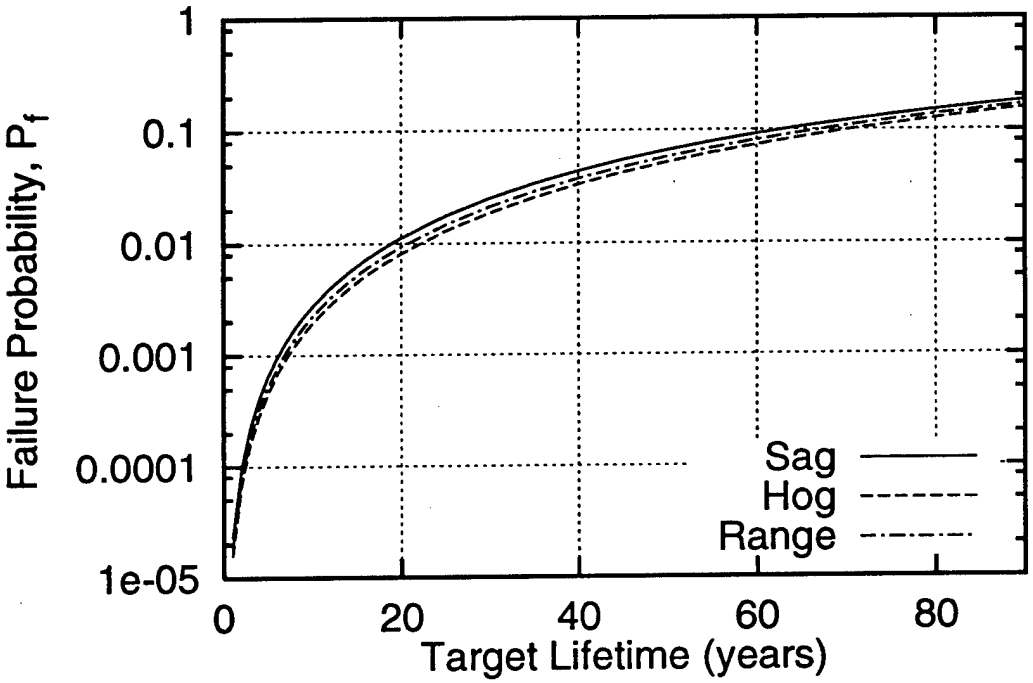

Figure 2.3: Failure probabilities for a range of target lifetimes for the three stresses: sag, hog and range

again is due to the nonlinearity in the stress to wave height relation where the sag stress amplifies the uncertainty contribution of the environment variables more than the hog stress. In the range case, the environment importance seems to be between the sag and hog cases.

In the next section, we illustrate how techniques based on FORM – in particular, the inverse FORM method – can be used in design of fatigue-sensitive components. For purposes of illustration, we focus on a two variable case which assumes only the values of SCF and of C to be uncertain. The general approach can be extended to a larger number of variables, however.

2.4 Selection of Material Properties in Design to Achieve Desired Reliability

In the previous section, we saw that the stress concentration factor SCF and the S–N factor C seemed be of most importance compared to the other associated random variables in the fatigue analysis (especially true in the hog stress case). Here we demonstrate a methodology to select the SCF and C values for an element design, assuming these two variables carry all of the importance. This selection is to be based on the objective of achieving a certain given reliability β in the fatigue design.

2.4.1 Forward FORM

We first restate the forward FORM problem, where the analysis proceeds as shown in the previous section for sag, hog and range stresses. Here, the distributions of SCF and C are specified and we find the resulting reliability level from FORM analysis. Eqn. 2.2 can be rewritten as

$$T_f = \frac{C\Delta}{f_0 \mathrm{SCF}^b E[S^b]} \tag{2.10}$$

in which we assumed $\overline{D}$ is given as $E[S^b]/C$ scaled by the SCF. In this example, we will model the only uncertain parameters, SCF and C, as independent lognormal variables:

$$\mathrm{SCF} = \breve{\mathrm{K}}\varepsilon_{\mathrm{SCF}}\ ; \quad C = \breve{C}\varepsilon_C \tag{2.11}$$

in which $\breve{\mathrm{K}}$ and $\breve{C}$ are the median values of the random variables SCF and C, respectively. $\varepsilon_{\mathrm{SCf}}$ and ε_C are unit median lognormal variables with coefficients of variation V_{SCF} and V_C, respectively. The remaining parameters in Eqn. 2.10 are assumed to be

deterministic. We can rewrite T_f as

$$T_f = \breve{T}_f \frac{\varepsilon_C}{\varepsilon^b_{\text{SCF}}} \tag{2.12}$$

in which $\breve{T}_f$ now indicates the median time to fail. Recall this was taken to be 200 years in the fatigue analysis example. Note that the assumption of only two variables that are independent and lognormally distributed is not critical here.

The $G(X)$ function 2.3 can be conveniently rewritten as

$$G(X) = \log\left(\frac{T_f}{T_t}\right) = \log\left(\frac{\breve{T}_f \varepsilon_C}{T_t \varepsilon^b_{\text{SCF}}}\right) = \log\left(\frac{\gamma \varepsilon_C}{\varepsilon^b_{\text{SCF}}}\right) \tag{2.13}$$

where $\gamma = \breve{T}_f / T_t$ is a ratio of a design lifetime to a specified service lifetime. Larger γ values indicate smaller service lifetimes compared to the design lifetime.

For the forward FORM problem, we choose $\gamma = 10$ implying the design life is 10 times the service life and assume $V_{\text{SCF}} = 0.1$, $V_C = 0.5$ (as in the earlier example). The S–N exponent $b = 6$, say. We find the failure probability to be $P_f = 1.27\times10^{-3}$ or reliability $\beta = 3.02$ and the design point is $\varepsilon^*_C = 0.41$, $\varepsilon^*_{\text{SCF}} = 1.267$. This says that we need to choose about 41% of the median C value (S–N curve) and should increase the median SCF by about 27% to get a β of 3.02. If we wish to use another material (another b value), we will need to rerun the forward FORM analysis to find the resulting reliability. This reliability will be different than 3.02, in general. Now, in a design scenario, where we wish to achieve a specified β value and then find the design point ε^*_C and $\varepsilon^*_{\text{SCF}}$ when using different materials, it is easier to solve the inverse FORM problem.

2.4.2 Inverse FORM

The idea of an inverse FORM analysis is to select the design parameters to achieve a certain given reliability β. This idea has been demonstrated earlier to provide environmental contours for structural response analysis [36] of offshore structures against ultimate collapse limit states. This idea also finds application in earthquake engineering [3] where magnitude-distance contours are provided for performing probabilistic seismic hazard analysis of structures.

The first issue in the inverse FORM analysis is to find the locus of all points in the normal U-space each of which would yield the same probability of failure for a failure state function passing through the point as a tangent line. This locus of points for the two-variable case happens to be a circle of radius β around the origin. This is shown in Fig. 2.4, where the dashed line indicates $G(X) = 0$. The circle in U-space (U_1, U_2) can be transformed to the physical space (ε_C and ε_{SCF}) by first transforming U_1 marginally and then conditionally transforming U_2 using the given distribution functions of the physical variables. The transformed circle is what we call as a "material" contour.

Note that the material contour only depends on the distributions of ε_C and ε_{SCF}. This contour can be estimated regardless of the S–N exponent b and regardless of the design life to service life ratio γ. Given this contour, one can now design against a worst-case scenario. In this case, we search along the contour for the largest possible γ (minimum fatigue life) for a desired b value. Usually the physics of the problem gives a good insight into where this design point might be on the contour, in which case the search can be localized to a smaller region.

For the example problem in this study, Fig. 2.5 shows the resulting material contour for SCF and C for a $P_f = 1.27\times10^{-3}$ ($\beta = 3.02$). Recall this was the

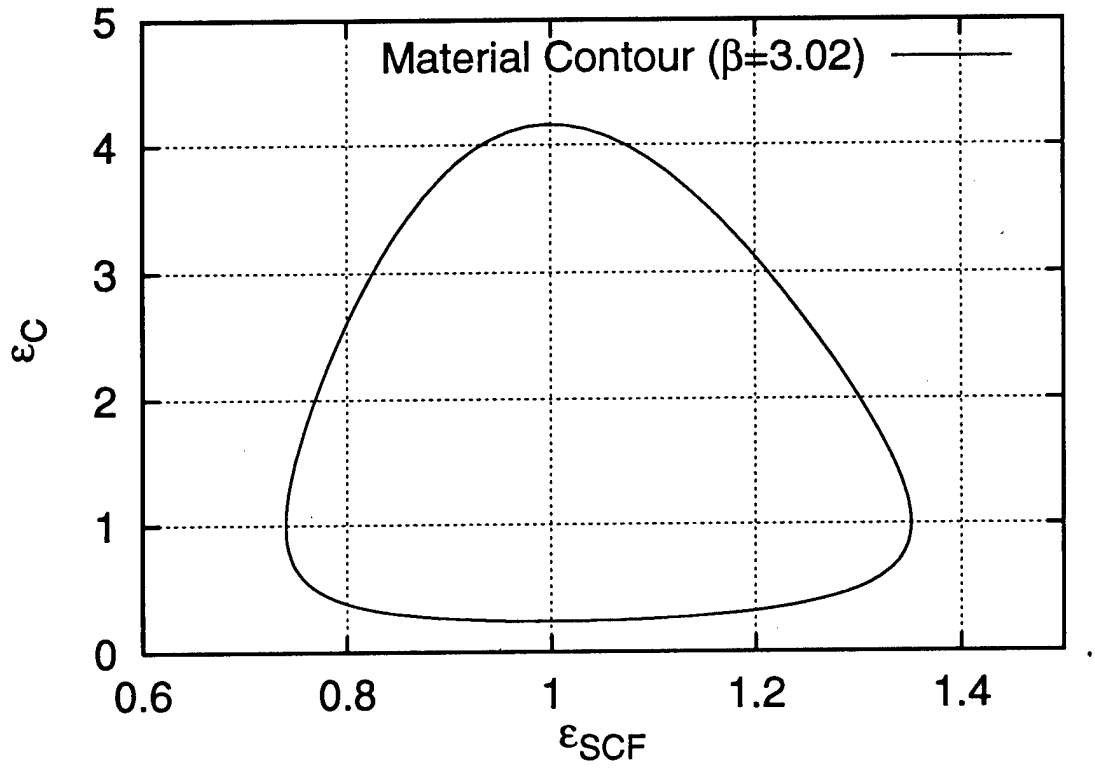

Figure 2.5: Material contour: Locus of points of ε_C and ε_{SCF} for which FORM method gives a reliability $\beta = 3.02$

to predict fatigue damage using the long-term distribution of the wave height H and periods T. Such a scheme can be easily implemented in the FORM analysis.

Alternatively, we could assume the ship load (mid-ship bending moment) to be the result of a second-order nonlinear system, and given the wave input seek to identify the first- and second-order transfer functions that define the system. Once these transfer functions are estimated, we can readily find the moment-influence coefficients (see Reference [15]: Eqns. 1.6 and 1.7) for the given seastate parameters (H_s, T_p). Using these moments, we can calibrate a distribution of the stresses and then find

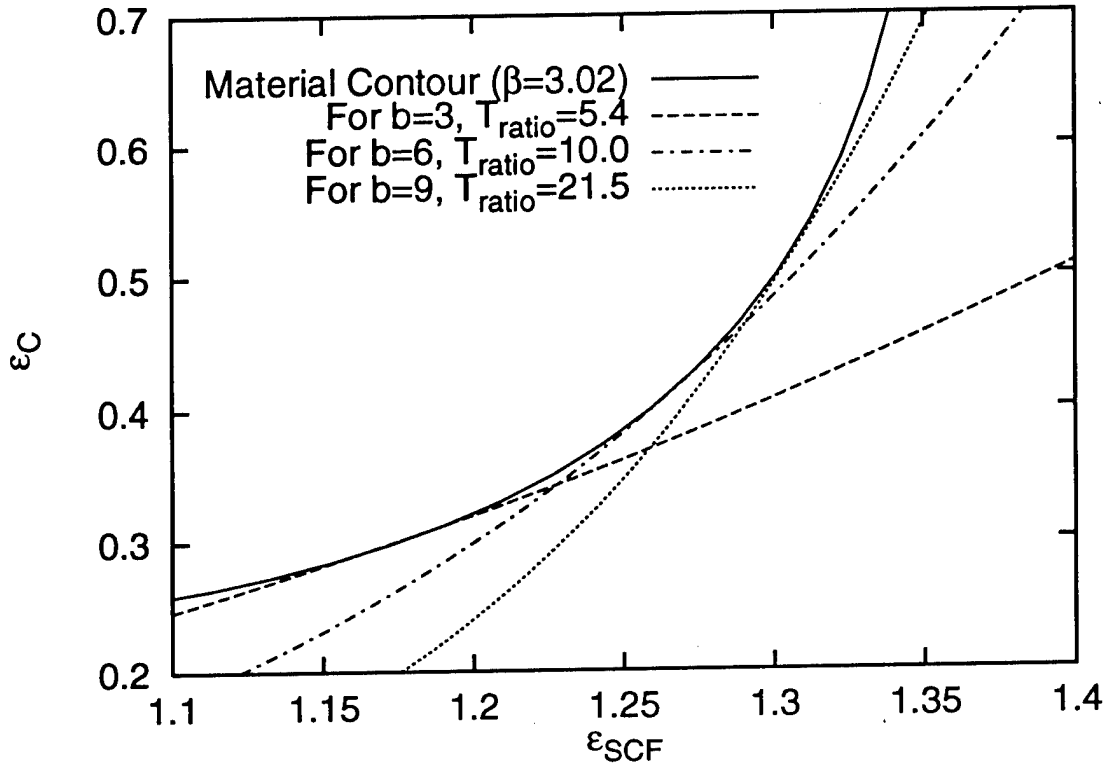

Figure 2.6: Design choices of ε_C and ε_{SCF} for different S–N exponents b that result in desired reliability $\beta = 3.02$

the resulting fatigue damage in this seastate. The long-term damage can be found by summing such damage estimates across a set of selected seastate parameters [31, 32]. These parameters may be selected, for example, at the quadrature points of the joint distribution of the parameters to efficiently calculate the long-term damage.

2.5.2 Future Work

In modeling the response (S) given the environment (H) denoted as "$S|H$", we chose the form $E[S|H] = aH^p$, in which a and p were found from regression analysis using

one hour of stress simulation in a specific seastate. This was the most damaging seastate according to a linear analysis. We suggest investigating the impact on P_f when using simulations in other seastates to estimate a and p.

Another suggestion is to extend the fatigue reliability analysis to include the NTF scheme to predict fatigue damage using the long-term distribution of the wave height H and periods T. Such a scheme can be easily implemented in the FORM analysis.

Alternatively, we could assume the ship load (mid-ship bending moment) to be the result of a second-order nonlinear system, and given the wave input seek to identify the first- and second-order transfer functions that define the system. Once these transfer functions are estimated, we can readily find the moment-influence coefficients (see [15]: Eqn. 1.6 and 1.7) for the given seastate parameters (H_s, T_p). Using these moments, we can calibrate a distribution of the stresses and then find the resulting fatigue damage in this seastate. The long-term damage can be found by summing such damage estimates across a set of selected seastate parameters [31, 32]. These parameters may be selected, for example, at the quadrature points of the joint distribution of the parameters to efficiently calculate the long-term damage.

Bibliography

[1] ABS. Guide for dynamic based design and evaluation of bulk carrier structures. Technical report, American Bureau of Shipping, New York, NY, USA, 1995.

[2] American Petroleum Institute. *Recommended Practice for Planning, Designing and Constructing Fixed Offshore Platforms - Load and Resistance Factor Design 2A-LRFD (RP 2A-LRFD)*, first edition edition, 1993.

[3] P. Bazzurro, S.R. Winterstein, T.C. Ude, and C.A. Cornell. Magnitude-distance contours for probabilistic seismic hazard analysis. In *7th ASCE Probabilistic Engineering Mechanics Conference*, Worcester, Massachusetts, 1996.

[4] R. F. Beck and A. Magee. *Developments in Marine Technology: 7: Dynamics of Marine Vehicles and Structures in Waves*, chapter Time-Domain Analysis for Predicting Ship Motions. Elsevier Science Publishers B. V., Amsterdam, 1991.

[5] T. Børresen. NV1418- time domain solution of large-amplitude ship motions in head seas: Users manual. Technical Report 81-0575, Det Norske Veritas, Oslo, Norway, 1981.

[6] A. Canavie, M. Arhan, and R. Ezraty. A statistical relationship between individual heights and periods of storm waves. In *Proceedings BOSS'76*, volume 2, Trondheim, Norway, 1976.

[7] DNVC. Fatigue assessment of ship structures. Technical Report 93-0432, Det Norske Veritas Classification AS, Høvik, Norway, 1994.

[8] Bitner-Gregersen E.M., E.H. Cramer, and R. Loseth. Uncertainties of load characteristics and fatigue damage of ship structures. In *Offshore Marine and Arctic Engineering OMAE, Safety and Reliability*, volume II, 1993.

[9] O. M. Faltinsen. *Sea Loads on Ships and Offshore Structures.* Cambridge University Press, 1990.

[10] G. Z. Forristall. On the statistical distribution of wave heights in a storm. *Journal of Geophysical Research*, 83(C5):2353–2358, 1978.

[11] F. Frimm. Implementation of irregular waves into program NV1418. Technical report, Veritas Marine Services (U.S.A), Inc., 1991.

[12] H. O. Fuchs and R. I. Stephens. *Metal Fatigue in Engineering.* John Wiley & Sons, 1980.

[13] P.F. Hansen and Winterstein S.R. Fatigue damage in the side shells of ships. *Marine Structures*, 8:631–655, 1995.

[14] S. Haver and K. A. Nyhus. A wave climate description for long term response calculations. In *Proceedings of the 5th OMAE Symposium*, number IV, pages 27–34. American Society of Mechanical Engineers, 1986.

[15] A. K. Jha. Nonlinear random ocean waves: Prediction and comparison with data. Technical Report RMS–24, Civil Engr. Dept., Stanford University, Reliability of Marine Structures, 1997.

[16] A. K. Jha. *Nonlinear stochastic models for loads and responses of offshore structures and vessels.* PhD thesis, Stanford University, 1997.

[17] A. K. Jha, C. H. Lange, and Winterstein S. R. Fatigue reliability: Formulation and analysis. Technical Report RMS–27, Civil Engineering Department, Stanford University, Reliability of Marine Structures, 1997.

[18] D. C. Kring. *Time Domain Ship Motions by a 3-Dimensional Rankine Panel Method.* PhD thesis, Massachusetts Institute of Technology, May 1994.

[19] W.-M. Lin, M. J. Meinhold, N. Salvesen, and D. K. P. Yue. Large-amplitude motions and wave loads for ship design. *20th Symposium on Naval Hydrodynamics*, August 1994.

[20] W. M. Lin and D. K. P. Yue. Numerical solutions for large-amplitude ship motions in the time domain. In *18th Symposium on Naval Hydrodynamics.* University of Michigan, Ann Arbor, MI, USA, 1990.

[21] G. Lindgren and I. Rychlik. Wave characteristic distributions for gaussian waves. *Ocean Engineering*, 9:411–432, 1982.

[22] M. S. Longuet-Higgins. On the joint distribution of the period and amplitude of sea waves. *Journal of Geophysical Research*, 80:2688–2694, 1975.

[23] M. S. Longuet-Higgins. On the joint distribution of wave periods and amplitudes in a random wave field. In *Proceedings of the Royal Society of London*, number A389, pages 241–258, April 1983.

[24] H. O. Madsen, S. Krenk, and N. C. Lind. *Methods of Structural Safety.* Prentice-Hall, Inc., New Jersey, 1986.

[25] T. Marthinsen and S. R. Winterstein. On the skewness of random surface waves. In *Proceedings of the 2nd International Offshore and Polar Engineering Conference, San Francisco*, pages 472–478. ISOPE, 1992.

[26] W. H. Munse, T. W. Wilbur, M. L. Tellalian, K. Nicoll, and K. Wilson. Fatigue characterization of fabricated ship details for design. Technical Report SR-1257, Ship Structure Committee, U.S. Coast Guard, Washington, D.C., August 1982.

[27] D. E. Nakos and P. D. Sclavounos. Ship motions by a three-dimensional rankine panel method. In *Proceedings of the 18th Symposium on Naval Hydrodynamics*, Ann Arbor, Michigan, 1990.

[28] W.H. Press, S.A. Teukolsky, W.T. Vetterling, and B.P. Flannery. *Numerical recipies in FORTRAN: The art of scientific computing.* Cambridge University Press, second edition edition, 1992.

[29] C. Sundararajan, editor. *Probabilistic Structural Mechanics Handbook: Theory and Industrial Applications.* Chapman & Hall, New York, 1995.

[30] R. Torgaus. *Extreme response of nonlinear ocean structures: Identification of minimal stochastic wave input for time-domain simulation.* PhD thesis, Stanford University, 1996.

[31] T. C. Ude. Second-order load and response models for floating structures: Probabilistics analysis and system identification. Technical Report RMS–16, Reliability of Marine Structures, Dept. of Civil Engr., Stanford University, 1994.

[32] T.C. Ude and S.R. Winterstein. Predicting fatigue damage matrices for floating structures across multiple seastates: The DamMat routine. Technical report, Civil Engr. Dept., Stanford University, 1996.

[33] WAVESHIP, 6.1. *Wave Loads on Slender Vessels – Users Manual.* Det Norske Veritas - SESAM, Høvik, Norway, 1993.

[34] T. Williams and C. Kelley. *GNUPLOT: Public-domain interactive plotting program.* Internet URL http://www.cs.dartmouth.edu/gnuplot_info.html.

[35] S. R. Winterstein. Nonlinear effects of ship bending in random seas. Technical Report 91-2032, Det Norske Veritas, Oslo, Norway, 1991.

[36] S.R. Winterstein, T.C. Ude, P. Bazzurro, and C.A. Cornell. Ocean environment contours for structural response analysis and experiment design. In *7th ASCE Probabilistic Engineering Mechanics Conference*, Worcester, Massachusetts, 1996.

REPORT DOCUMENTATION PAGE

Form Approved
OMB No. 0704-0188

1. REPORT DATE (DD-MM-YYYY)	2. REPORT DATE	3. DATES COVERED (From - To)
00-06-1997	June, 1997	

4. TITLE AND SUBTITLE
Nonlinear Ship Loads and Fatigue Reliability

5a. CONTRACT NUMBER

5b. GRANT NUMBER
N00014-96-1-0641

5c. PROGRAM ELEMENT NUMBER

6. AUTHOR(S)
Alok K. Jha

5d. PROJECT NUMBER

5e. TASK NUMBER

5f. WORK UNIT NUMBER

7. PEREORMING ORGANIZATION NAME(S) AND ADDRESS(ES)
RMS Group
S.R Winterstein, C.A. Cornell
Blume Center
Stanford University, CA 94305

8. PERFORMING ORGANIZATION REPORT NUMBER
RMS-26

9. SPONSORING/MONITORING AGENCY NAME(S) AND ADDRESS(ES)
OFFICE OF NAVAL RESEARCH
800 N. QUINCY ST.
ARLINGTON, VA 22217-4620
ATTN: RASHDY BARSOUM

10. SPONSOR/MONITOR'S ACRONYM(S)

11. SPONSORING/MONITORING AGENCY REPORT NUMBER

12. DISTRIBUTION AVAILABILITY STATEMENT
APPROVED FOR PUBLIC RELEASE

13. SUPPLEMENTARY NOTES

14. ABSTRACT
Stochastic methods are described to predict the effects of nonlinear ship loads on fatigue accumulation in random seas. These are found to be a computationally efficient means of predicting net fatigue damage over many ship fatigue cycles. First order reliability Method (FORM), and Narrow Band Transfer function (NTF) methods are applied. The results are compared with full non-linear analysis of a specific ship over long simulations of an irregular sea. Finally, a fatigue reliability example is presented in which the probability of failure is found by integrating over: wave climate, structural response and material properties.

15. SUBJECT TERMS

16. SECURITY CLASSIFICATION OF:			17. LIMITATION OF ABSTRACT	18. NUMBER OF PAGES	19a. NAME OF RESPONSIBLE PERSON
a. REPORT	b. ABSTRACT	c. THIS PAGE			19b. TELEPONE NUMBER (*Include area code*)